HHS Public Access

Author manuscript

Cell Chem Biol. Author manuscript; available in PMC 2020 May 16.

Published in final edited form as:

Cell Chem Biol. 2019 May 16; 26(5): 674–685.e6. doi:10.1016/j.chembiol.2019.02.002.

Covalent Modification and Regulation of the Nuclear Receptor Nurr1 by a Dopamine Metabolite

John M. Bruning[1], **Yan Wang**[2], **Francesca Oltrabella**[3], **Boxue Tian**[2], **Svetlana A. Kholodar**[2], **Harrison Liu**[4], **Paulomi Bhattacharya**[2], **Su Guo**[3], **James M. Holton**[5], **Robert J. Fletterick**[5], **Matthew P. Jacobson**[2,3], **Pamela M. England**[2,6,7,*]

[1]Pharmaceutical Sciences and Pharmacogenomics Graduate Program, University of California San Francisco, San Francisco, California 94158, USA

[2]Department of Pharmaceutical Chemistry, University of California San Francisco, San Francisco, California 94158, USA

[3]Department of Bioengineering and Therapeutic Sciences, University of California San Francisco, San Francisco, California 94158, USA

[4]Bioengineering Graduate Program, University of California San Francisco, San Francisco, California 94158, USA

[5]Department of Biochemistry and Biophysics, University of California San Francisco, San Francisco, California 94158, USA

[6]Department of Cellular and Molecular Pharmacology, University of California San Francisco, San Francisco, California 94158, USA

[7]Lead Contact

Abstract

Nurr1, a nuclear receptor essential for the development, maintenance, and survival of midbrain dopaminergic neurons, is a potential therapeutic target for Parkinson's disease, a neurological disorder characterized by the degeneration of these same neurons. Efforts to identify Nurr1 agonists have been hampered by the recognition that it lacks several classic regulatory elements of nuclear receptor function, including the canonical ligand-binding pocket. Here we report that the

*Correspondence: pamela.england@ucsf.edu.

AUTHOR CONTRIBUTIONS

Biophysical assays, molecular modeling, and crystallography were performed by J.B.; quantum mechanical calculations were performed by B.T.; cell-based assays were performed by Y.W. and P.B.; preparation of mutant protein was performed by S.K.; zebrafish assays were performed by F.O. and H.L.

DATA AND SOFTWARE AVAILABILITY

The coordinates for Nurr1 LBD dopamine metabolite complex structure have been deposited in the protein data bank (PDB) under the ID code 6DDA.

DECLARATION OF INTERESTS

M.P.J. is a consultant to and shareholder of Schrodinger Inc., which develops, licenses and distributes some of the software used in this work.

dopamine metabolite 5,6-dihydroxyindole (DHI) binds directly to and modulates the activity of Nurr1. Using biophysical assays and x-ray crystallography we show that DHI binds to the ligand binding domain within a non-canonical pocket, forming a covalent adduct with Cys566. In cultured cells and zebrafish, DHI stimulates Nurr1 activity, including the transcription of target genes underlying dopamine homeostasis. These findings suggest avenues for developing synthetic Nurr1 ligands to ameliorate the symptoms and progression of Parkinson's disease.

Graphical abstract

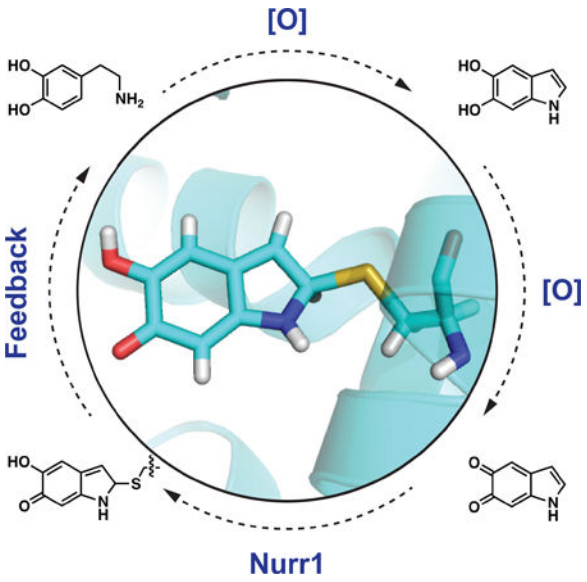

eTOC Blurb

Nurr1, a critical regulator of dopaminergic neuron health and potential therapeutic target for Parkinson's disease, lacks the canonical nuclear receptor ligand binding pocket. Here, Bruning et al. demonstrate that the receptor binds to a dopamine metabolite and show that the metabolite drives the expression of cellular machinery underlying dopamine homeostasis.

INTRODUCTION

Parkinson's disease (PD) is a neurological disorder afflicting 10 million people worldwide (Wirdefeldt et al., 2011). In an estimated 90% of PD patients, the cause of the disease is unknown, having no clear genetic or environmental origin (de Lau and Breteler, 2006). The most pronounced neuropathological feature of PD is the progressive degeneration of dopaminergic neurons in the substantia nigra pars compacta and the consequent reduction in dopamine levels in the striatum, which manifest as impairments in motor function (e.g. rigidity, tremor, bradykinesia) (Samii et al., 2004). Notably, this degeneration appears to be *preceded* by the loss of the dopaminergic phenotype; that is, at least some dopaminergic neurons first stop producing and signaling with dopamine prior to degenerating (Janezic et al., 2013). Although the molecular basis for idiopathic PD remains incompletely understood, it has been proposed to include oxidative stress, mitochondrial dysfunction, and dysregulation of dopamine homeostasis (Blesa et al., 2015; Hauser and Hastings, 2013;

Hwang, 2013). Currently, there are no available treatments that stop or even slow the progression of PD. Existing therapeutics relieve PD symptoms by increasing dopaminergic signaling through one of three mechanisms: (1) increasing dopamine levels by augmenting the amount of its biosynthetic precursor, L-DOPA; (2) blocking the breakdown of dopamine by inhibiting its metabolic enzymes (MAO, COMT); (3) mimicking the activity of dopamine by directly agonizing dopamine receptors. However, these drugs only partially alleviate symptoms and can have significant side effects, especially as the disease progresses. New types of therapeutics are desperately needed to combat both the symptoms and progression of PD.

The nuclear receptor related-1 protein, Nurr1 (NR4A2), is a transcription factor that regulates the expression of genes critical for the development, maintenance, and survival of dopaminergic neurons (Alavian et al., 2014; Decressac et al., 2013; Dong et al., 2016; Jankovic et al., 2005; Johnson et al., 2011; Kadkhodaei et al., 2009; Luo, 2012; Zetterstrom et al., 1997). In particular, Nurr1 plays a fundamental role in maintaining dopamine homeostasis by regulating transcription of the genes governing dopamine synthesis (*TH*, tyrosine hydroxylase; *DDC*, dopa decarboxylase), packaging (*SLC18A2*, vesicular monoamine transporter 2, VMAT2), and reuptake (*DAT*, dopamine transporter, also known as *SLC6A3*)(Hermanson et al., 2003; Iwawaki et al., 2000; Johnson et al., 2011; Sacchetti et al., 2001) (Figure 1A). Nurr1 also regulates the survival of dopaminergic neurons by stimulating the transcription of genes coding for neurotrophic factors (BDNF, NGF), anti-inflammatory responses (GDNF receptor c-Ret), and oxidative stress management (SOD1), as well as repressing the transcription of pro-inflammatory genes (TNFalpha, iNOS, IL-1beta) (Galleguillos et al., 2010; Johnson et al., 2011; Kadkhodaei et al., 2013; Kim et al., 2003; Saijo et al., 2009; Sakurada et al., 1999; Volpicelli et al., 2007). Validation of Nurr1 as a PD therapeutic is primarily derived from mouse models and human data. Homozygous mice lacking Nurr1 fail to generate midbrain dopaminergic neurons and die shortly after birth, heterozygous mice have motor impairments analogous to Parkinsonian deficits, and conditional ablation of Nurr1 in adult animals recapitulates early features of PD with progressive dopaminergic neuropathology (Jiang et al., 2005; Kadkhodaei et al., 2013; Kadkhodaei et al., 2009; Zetterstrom et al., 1997; Zhang et al., 2012a). In patients with PD, the expression of Nurr1 is reduced compared to age-matched controls (Chu et al., 2006; Le et al., 2008; Montarolo et al., 2016; Moran et al., 2007), though only a few, rare polymorphisms in Nurr1 appear to be associated with the disease (Grimes et al., 2006; Le et al., 2003). Stimulation of Nurr1 activity may combat both the reduced dopamine levels and the increased oxidative stress associated with PD.

Efforts to identify Nurr1 agonists have been hampered by major gaps in our understanding of the receptor's structure and regulation. In particular, the only reported crystal structure of the receptor (apo Nurr1), published over 15 years ago, reveals the canonical nuclear receptor (NR) ligand binding pocket is filled by bulky amino acid side chains (Wang et al., 2003). Subsequent efforts to identify ligand binding sites within Nurr1, utilizing NMR studies of the isolated ligand binding domain (LBD), have suggested that small molecules may bind to the receptor in regions corresponding to both canonical and non-canonical ligand binding pockets (de Vera et al., 2016; Kim et al., 2015; Poppe et al., 2007). Phenotypic assays have identified a small number of synthetic ligands that reportedly up-regulate transcription and

protein levels of Nurr1 target genes, provide some degree of neuroprotection, and improve behavioral deficits in mouse models (Dong et al., 2016; Kim et al., 2015; McFarland et al., 2013; Smith et al., 2015; Zhang et al., 2012b). However, there is little evidence that any of these ligands directly activate endogenous Nurr1, with the exception of the antimalarial drug amodiaquine (Kim et al., 2015). Endogeneous ligands for Nurr1 have yet to be reported, further limiting our understanding of how this receptor is regulated. Efforts to drug Nurr1 indirectly by targeting the RXR ligand binding domain in Nurr1:RXR heterodimers have demonstrated enhanced expression of Nurr1 target genes by RXR agonists (McFarland et al., 2013; Spathis et al., 2017; Volakakis et al., 2015). This approach may, however, be limited by the established promiscuous association of RXR with other NRs (e.g. RAR, VDR, TR, PPAR, LXR, FXR), and complicated by the apparent repression of Nurr1 transcriptional activity upon complexation with RXR (Perez et al., 2012; Perlmann and Jansson, 1995). The receptor also lacks the canonical co-regulator binding groove, though some reports suggest alternative interaction surfaces for regulatory proteins may be present on the Nurr1 LBD (Codina et al., 2004; de Vera et al., 2016; Volakakis et al., 2006).

Against this backdrop, we set out to identify synthetic and endogenous ligands that bind directly to and regulate the activity of Nurr1. Owing to the pivotal role Nurr1 plays in producing and processing dopamine, and the need for neurons to tightly regulate dopamine levels, we postulated that the receptor might be regulated by dopamine, its biosynthetic precursor L-DOPA, or metabolites of these molecules (Figure 1B). Outside of an acidic environment (e.g. synaptic vesicle), dopamine is unstable (Segura-Aguilar et al., 2014). Following release into the synaptic cleft, excess dopamine is rapidly taken back up into the nerve terminal, traveling through the dopamine transporter, and then repacked into synaptic vesicles, via the vesicular monoamine transporter. Dopamine that is not processed in this way is typically either enzymatically (COMT, MAO) converted to inactive (but oxidatively unstable) metabolites or auto-oxidized into reactive species, including 5,6-dihydroxyindole (DHI) and 5,6-indolequinone (IQ) (Figure 1B), which are the focus of this work (Meiser et al., 2013). The reactive compounds polymerize to form neuromelanin, a chromogenic pigment of uncertain function that accumulates in and stains midbrain dopaminergic neurons black in healthy individuals (Fedorow et al., 2006; Zucca et al., 2017), or are otherwise quenched by direct conjugation to scavenging small molecules (e.g. glutathione) or protein thiols (Sulzer and Zecca, 2000). Using biophysical, structural, and biological assays, we evaluated the interaction of Nurr1 with oxidative metabolites of L-DOPA and dopamine. We found that DHI binds directly to Nurr1 in a non-canonical ligand binding pocket, forming a covalent adduct by reacting as the indolequinone (IQ) with an endogenous cysteine residue (Cys566). In both cultured cells and zebrafish, DHI stimulates Nurr1 transcription, including upregulating the target gene underlying the management of excess cytoplasmic dopamine (i.e. VMAT2).

RESULTS

DHI Binds Directly to the Nurr1 Ligand Binding Domain

Differential scanning fluorimetry (DSF) is a fluorescence-based thermal shift assay frequently used to identify specific interactions between small molecules and proteins

(Niesen et al., 2007); compounds that bind directly to and stabilize a protein typically increase the melting temperature (Tm). Using DSF, we found that DHI produces a concentration-dependent increase (1°C at 50 μM) in the Tm of the Nurr1 ligand bindin g domain (LBD) (Figure 2A, C), whereas even the structurally related C2-substituted metabolite 5,6-dihydroxyindole carboxylic acid (DHICA) does not alter the Tm (Figure 2B, D). DHI binding is detected at concentrations above 5–10 μM and there is some evidence of site saturation at the highest concentration tested (50 μM); it was not possible to obtain data at higher concentrations due to apparent polymerization of DHI, which is accelerated upon heating. We also observed that DHI, but not DHICA, produces a concentration-dependent decrease in the overall fluorescence, possibly due to precipitation of the protein caused by DHI polymers (Figure S1).

We confirmed direct binding of DHI to the Nurr1 LBD using surface plasmon resonance (SPR). Biotinylated Nurr1 LBD was immobilized on a biotin-capturing chip and screened against increasing concentrations of mobile analytes. As above, DHI (but not DHICA, dopamine, or L-DOPA; Figure S2), binds at micromolar concentrations directly to Nurr1 in a concentration-dependent manner and with kinetic features suggestive of a covalent interaction (Figure 3A). In particular, rather than exhibiting step-like ‘fast-on, fast-off’ kinetics typical of reversible small molecule (< 300 Da) binding, DHI appears to not dissociate from the receptor on the timescale of minutes, under these conditions.

To better characterize the kinetics of the DHI-Nurr1 interaction, we performed an additional SPR experiment in which the surface of the chip was regenerated (replacing the Nurr1 LBD) after each exposure to DHI to ensure that each response reflects DHI binding to naïve apo Nurr1 LBD. (Figure 3B). These experiments confirm that DHI exhibits the features of a specific, covalent binding event to Nurr1 by showing (i) a concentration-dependent increase in association rate, (ii) convergence of the association towards steady state at the highest concentration tested (2.5 μM; 320 s contact time), (iii) maximal association responses consistent with the theoretical maximal response (Rmax[1]) for one or possibly two molecules of DHI binding to each Nurr1 LBD, ruling out super-stoichiometric, non-specific binding.

As DHI and DHICA have been shown to form covalent adducts with cysteine, including in the process of pheomelanin formation (d’Ischia et al., 2005; Dischia et al., 1987; Mason and Peterson, 1965), we hypothesized that DHI might bind covalently to the Nurr1 LBD through one of its five conserved cysteine residues (Table S1). Consistent with this hypothesis, SPR experiments show that DHI binding to Nurr1 is reduced in the Cys566Thr and Cys465Ala mutants, but not in Cys505Thr, Cys534Thr, or Cys475 mutants (Figure 3C). Neither the Cys566Thr nor the Cys465Ala mutation eliminated DHI binding, suggesting that DHI binds to both Cys566 and Cys465. Examples of other electrophilic nuclear receptor ligands that also react with more than one cysteine residue have been previously reported (Reese et al., 1992). Unfortunately, we were not able to detect the DHI modification by mass spectroscopy, consistent with previous reports showing that “dopamine-modified” proteins (i.e. proteins exposed to dopamine under oxidizing conditions) could not be detected by

[1]Rmax is the maximum analyte (DHI) binding capacity of the immobilized ligand (Nurr1 LBD) expressed in resonance units (RU); see Experimental Procedures for additional information.

mass spectroscopy (Armarego and Waring, 1983; Belluzzi et al., 2012; Bisaglia et al., 2007; Girotto et al., 2012; Hastings, 2009; Kuhn et al., 1999; LaVoie et al., 2005; Whitehead et al., 2001). It is possible that the ionization process drives the neutral loss of these adducts and/or that the adducts are chemically reversible. Indeed, the reversibility of protein thiol Michael additions to drugs with enone systems has been previously observed (Lee et al., 2002). Unfortunately, Nurr1 LBD with four or five of the five cysteine residues mutated could not be expressed and/or purified, making it difficult to unambiguously determine the site or sites of DHI binding in this manner. As discussed below, we confirmed specific binding of DHI to Cys566 by x-ray crystallography, but cannot rule out binding to a secondary site, most likely Cys465. Notably, Cys465 is oxidized in one of the three chains in the x-ray structure (Figure S3), the biological significance of which is worthy of further exploration.

The Quinone Form of DHI Binds to the Nurr1 LBD within a Non-Canonical Ligand Binding Pocket

We characterized the structure of the Nurr1 LBD co-crystalized with DHI at the atomic scale using protein crystallography. The structure of the complex, determined at 3.2 Å resolution (PDB: 6DDA; Table S2), reveals that the metabolite binding site sits adjacent to the canonical ligand binding pocket[2], and confirms the modification of Cys566 (Figure 4). Structural alignment of the peptide backbones for liganded and apo Nurr1 LBD (pdb: 1OVL) reveals an overall Cα RMSD of 0.57 Å and highlights two important differe nces between the structures (Figure 4A). First, Cys566 appears in two distinct rotameric conformations in the structures; in the apo structure the thiol points towards the vestigial canonical ligand binding pocket, whereas in the liganded structure it points towards a pocket formed by H11, H12, and the bend in the middle of H4/5. Second, a 1.5 Å positional shift is observed between the two structures at the end of H12, a classic regulatory element among NRs. Otherwise, the two structures are very similar.

To enhance the signal of the ligand electron density, we generated Polder difference maps, which take into consideration bulk-solvent flattening effects that traditional OMIT maps do not (Figure 4B, Table S3). The ligand density is most consistent with a covalent bond between the Cys566 sulfur atom and C2 atom of IQ, the auto-oxidation product of DHI (Figure 4C); this density is not observed surrounding any of the other cysteine residues in the protein (Figure S3) Modeling with IQ attached via the C3, C4 or C7 atoms, which have previously been shown to be reactive sites (d'Ischia et al., 2011; d'Ischia et al., 1987), not only fit the ligand density more poorly, but also generated unavoidable steric clashes with protein side chains in the pocket.

Since it is not possible to unequivocally conclude from the electron density map that the metabolite is bound as the quinone, we employed quantum mechanical calculations to characterize the transition states and energy barriers for thiolate attack with both redox states (DHI and IQ) at each of the possible electrophilic sites (C2, C3, C4, C7). These studies revealed that the IQ C2-adduct is the most likely reaction product. Reaction between the thiolate and quinone species (IQ) at positions 2, 4 and 7 are all predicted to generate stable

[2]The term "canonical ligand binding pocket" refers to the expected site of ligand binding based on the classic binding pocket for ligands in well-characterized NRs, such as androgen, estrogen, and glucocorticoid receptors.

adducts, with transition state energy barriers of 6.3, 14.7 and 16.7 kcal/mol, respectively, relative to the reactants, whereas reaction at C3 is predicted to be unfavorable as the energies for the transition state and the corresponding product are both high (E_{act} > 30.0 kcal/mol) (Figure S4). Interestingly, the barrier to dissociation of the C2-quinone adduct is only ~3 kcal/mol, suggesting that the covalent adduct could be reversible under some conditions. Reaction between the thiolate and the catechol species (DHI) is unlikely, as all four adducts are predicted to be high-energy, unstable states that would spontaneously dissociate (Figure S5).

Modeling of the IQ C2-adduct into the electron density reveals that several intermolecular interactions are expected to stabilize the binding of DHI/IQ, and the covalent IQ-protein complex, including: i) hydrogen bonds between the guanidinium of Arg515 (H8–9 loop) and the C5 and C6 oxygens of DHI and IQ; ii) a hydrogen bond between the carboxylate of E445 (H4/5) and the NH of DHI and IQ; iii) a cation-pi interaction between Arg515 and/or Arg563 (H11) and the pi systems of DHI and IQ[3] (Figure 4B). One or both of these arginine residues may also stabilize formation of the oxyanion resulting from nucleophilic attack of the thiol. In the apo Nurr1 LBD structure the DHI/IQ binding site is occupied by ordered water molecules (two-four, depending on the chain); the release of these waters back into the bulk solvent (i.e. receptor desolvation) is entropically favorable and may also contribute to the initial non-covalent binding event. These interactions may also explain the preferential binding of DHI over DHICA; the latter contains a C2-carboxylate that renders it too big to fit within the metabolite pocket. An unresolved question in this work is whether DHI first autooxidizes to IQ in solution, after binding non-covalently to Nurr1 near Cys566, or both; the extreme instability of IQ makes it challenging to study. As noted, many of the favorable interactions observed in the IQ-Nurr1 adduct crystal structure would also stabilize non-covalent interactions with DHI, and we speculate that the positive charges of Arg515 and Arg563 might decrease the pKa of DHI hydroxyl groups, increasing its rate of oxidation to IQ, which generates two protons.

DHI Stimulates Nurr1 Activity

To probe the effect of DHI on the activity of Nurr1 in cultured cells, we utilized a reporter assay in which the NR LBD is fused to the Gal4 DBD, and binding of the chimeric protein to a reporter plasmid sequence (UAS cis-element) drives the expression of firefly luciferase (Castro et al., 1999). For these assays, JEG3 cells were co-transfected with an expression plasmid encoding the wildtype Nurr1 LBD fused to the Gal4 DBD (pM-Nurr1-Gal4) or the Gal4 DBD alone (pM-Gal4), along with a reporter plasmid (pGL4.35) encoding the firefly luciferase gene driven by an upstream 9×Gal4, and an internal control plasmid (pRL-TK) expressing renilla luciferase. Transfected cells were incubated with DHI, DHICA, or DMSO control for 6 h before luciferase signals were measured. In these assays, DHI produces a concentration-dependent increase in firefly luciferase expression, with a statistically significant effect at 10 μM DHI, and a 1.6-fold over basal increase in activation at 100 μM DHI (Figure 5). Basal activation is seen in the absence of DHI and DHICA (i.e. DMSO

[3]A cation-pi interaction between arginine and tryptophan (indole) residues is frequently observed in structural biology; over one-fourth of the tryptophans in the protein data bank experience an energetically significant cation-pi interaction (see Gallivan and Dougherty, 1999).

only), in agreement with the constitutive Nurr1 activation reported by others (Castro et al., 1999; Wang et al., 2003). Concentrations of DHI above 100 μM were cytotoxic, preventing us from obtaining an EC_{50}.

To study the effect of DHI on the activity of Nurr1 in neurons, we characterized the transcription of several Nurr1 target genes in zebrafish, a model organism that has been used for studying Parkinson's disease (Xi et al., 2011; Zhang et al., 2017). The zebrafish genome encodes two isoforms of Nurr1, the NR4A2A isoform expressed predominantly in dopaminergic neurons and the NR4A2B isoform expressed predominantly in the eye (Blin et al., 2008). The LBD of the neuronal isoform has remarkably high sequence identity, 95%, with the human Nurr1 LBD, and all of the cysteine residues are conserved (Table S1). In these assays, zebrafish embryos three days post-fertilization (3 dpf) were exposed to DHI for either 6 h or 24 h, after which RNA was extracted and subjected to RT-qPCR analysis (Figure 6). At 6 h post treatment with 100 μM DHI, only the transcript levels of genes coding for the transporters of dopamine (*vmat2*, *dat*) show statistically significant increases (Figure 6A). At 24 h post-treatment, the increased expression of *vmat2* remains significant, and there are also statistically significant increases in the transcript levels for the rate-limiting biosynthetic enzyme tyrosine hydroxylase (*th*) (Figure 6B).

DISCUSSION

Considerable evidence suggests that dysregulation of dopamine is both a contributor to and consequence of PD (Burbulla et al., 2017; Hastings, 2009; Jenner, 2003; Lotharius and Brundin, 2002; Sulzer et al., 2000). Metabolism of dopamine produces reactive oxygen species (ROS) and quinones, and the formation of these toxins is exacerbated by excessive levels of cytoplasmic dopamine (VMAT2 dysfunction), increased levels of ROS (mitochondrial dysfunction), and other forms of oxidative stress—a ll conditions associated with PD. The transcriptional regulator Nurr1 plays a pivotal role in maintaining dopamine homeostasis, regulating the synthesis, packaging, and re-uptake of the neurotransmitter. The regulation of Nurr1 itself is incompletely understood, however, partly owing to the absence of a well-defined ligand binding pocket within the receptor. Delineating a binding site for small molecules within Nurr1 is a critical step toward understanding this receptor's role in and potential effect on PD.

In this study, we used biophysical and structural assays to identify a binding site for a specific dopamine metabolite within the Nurr1 LBD. We found that 5,6-dihyroxyindole (DHI) binds to Nurr1 within a non-canonical binding site, forming a covalent adduct as the indolequinone (IQ) with Cys566. The interaction with DHI/IQ is detectable by surface plasmon resonance in the high nanomolar range (>0.25 μM), a concentration consistent with sensing cytoplasmic dopamine under conditions of oxidative stress (Eisenhofer et al., 2004; Mosharov et al., 2003; Mosharov et al., 2006; Olefirowicz and Ewing, 1990; Omiatek et al., 2013; Pifl et al., 2014), and starts to show evidence of saturable binding at low micromolar concentrations (2.5 μM, Figure 3). In functional assays, DHI stimulates Nurr1 activity, driving the transcription of genes controlling dopamine homeostasis. These data suggest that Nurr1 functions as a sensor for oxidative stress in dopaminergic neurons, responding directly to a specific oxidative metabolite of dopamine.

DHI Binds to Nurr1 within a Regulatory Hotspot

Nuclear receptors are highly modular structures, typically with multiple surfaces engaging in protein-protein interactions and accessibility to these sites allosterically regulated by the binding of small molecules within the LBD (Gallastegui et al., 2015; Gronemeyer et al., 2004; Huang et al., 2010; Kumar and McEwan, 2012). Consistent with this established view of NR regulation, the DHI/IQ binding site is situated among several regulatory surfaces and metabolite binding produces a structural change in H12, a key regulator of NR function (Figure 7). In particular, metabolite binding produces 1.5 Å shift in H12 that potentially impacts the binding of co-regulator proteins (Codina et al., 2004), nuclear export of the receptor (Garcia-Yague et al., 2013), homodimerization with Nurr1 (Zhan et al., 2012), and heterodimerization with RXR (Aarnisalo et al., 2002).

The conformational changes affected by DHI/IQ appear to alter the activity of Nurr1, upregulating the expression of Nurr1 target genes. Nurr1 reportedly signals as a monomer, homodimer, and heterodimer in neurons, with each conformation recognizing distinct DNA response elements and thus regulating transcription of different target genes (Maira et al., 1999; Paulsen et al., 1995; Perlmann and Jansson, 1995; Philips et al., 1997; Volpicelli et al., 2012; Zetterstrom et al., 1996). Our data suggests that DHI/IQ binding to Nurr1 biases the oligomerization state of the receptor toward the monomer, as two of the genes upregulated by the metabolite (*vmat2* and *th*) both contain promoter sequences that are recognized by full-length Nurr1 monomers (i.e. NBRE and NBRE-like response elements).[4]

Nurr1 Senses and Responds to Oxidative Stress

A number of studies have shown that auto-oxidized dopamine metabolites can covalently modify proteins intimately involved in PD, such as SOD2, TH, DJ1, DAT, DHPR, alpha-synuclein, and parkin (Armarego and Waring, 1983; Belluzzi et al., 2012; Bisaglia et al., 2007; Girotto et al., 2012; Hastings, 2009; Kuhn et al., 1999; LaVoie et al., 2005; Whitehead et al., 2001). In all of these cases, the modifications inhibit normal protein function, often by driving the formation of higher order protein species (e.g. crosslinked protein) and/or by reducing protein stability.[5] In contrast, here we provide an example of a specific protein modification by a dopamine metabolite that stimulates function.

We observed that acute (6 h) treatment of zebrafish with DHI stimulates the transcription of genes underlying the reuptake and packing of dopamine (*dat*, *vmat2*), whereas prolonged (24 h) treatment stimulates transcription of genes underlying the synthesis and packaging genes (*th*, *vmat2*). The observed upregulation of VMAT2 gene transcripts is particularly interesting as the functioning of this vesicular transporter is an important determinant of dopamine-related oxidative stress, neurodegeneration, and PD (Alter et al., 2013; Guillot and Miller, 2009). For example, reduced vesicular storage of dopamine has been shown to result in progressive neurodegeneration in mouse models (Caudle et al., 2007; Chen et al., 2008; Ulusoy et al., 2012). Furthermore, defects in VMAT2 function are observed in synaptic

[4]We assume that the promoter sequences in zebrafish are similar to those identified in mammals.
[5]In these examples, the specific modifications could not be unambiguously identified, as the reactive metabolites were generated by treating dopamine with tyrosinase or chemical oxidants (i.e. $NaIO_4$, H_2O_2), resulting in the production of several different reactive species (e.g., see Figure 1B).

vesicles isolated from the striatum of patients with PD (Pifl et al., 2014). Conversely, a gain of function VMAT2 haplotype in humans has been shown to be protective in PD (Brighina et al., 2013; Glatt et al., 2006) and upregulation of VMAT2 in mouse models of PD has been shown to provide protection against neurodegeneration (Lohr et al., 2014). Finally, drugs that inhibit VMAT2 function or otherwise increase levels of cytoplasmic dopamine (e.g. methamphetamine, cocaine) are associated with degeneration of dopaminergic neurons and increased risk for PD (Guillot et al., 2008; Krasnova and Cadet, 2009). Thus, in addition to its fundamental role in neurotransmission, VMAT2 also plays a neuroprotective role by sequestering dopamine in acidic synaptic vesicles.

Nurr1 is a Ligand-inducible Transcription Factor

Although Nurr1 is widely recognized as a therapeutic target for PD, the absence of a well-defined ligand binding pocket has hampered efforts to capitalize on this potential. Previous reports have hinted at canonical and non-canonical ligand binding sites within the Nurr1 LBD (Figure S6) (de Vera et al., 2016; Kim et al., 2015; Poppe et al., 2007). The binding site for DHI/IQ is most closely approximated by Poppe et al., who highlighted the proximity of Cys566 to a binding site for benzimidazole-containing compounds. Additional x-ray structures of liganded Nurr1 further underscore the existence of multiple small molecule binding sites within the LBD (manuscript in preparation).

Our findings demonstrate that Nurr1 is a ligand-inducible transcription factor. While DHI itself is an unstable molecule, auto-oxidizing and polymerizing with itself and other dopamine metabolites, the indole core is a tractable scaffold for developing stable compounds targeting Nurr1. Further, the reactivity of Cys566 suggests avenues for developing both reversible and irreversible covalent compounds targeting the receptor. Such compounds could impact the progression and symptoms of PD. Improving the packaging of dopamine into vesicles by upregulating transcription of VMAT2 may slow the progression of Parkinson’s disease, and extend the treatment window for L-DOPA by reducing side-effects. Increasing the synthesis of dopamine by upregulating transcription of the rate limiting biosynthetic enzyme, TH, offers an orthogonal method for increasing dopamine levels.

STAR METHODS

CONTACT FOR REAGENT AND RESOURCE SHARING

Further information and requests for resources and reagents should be directed to and will be fulfilled by Pamela M. England (pamela.england@ucsf.edu)

EXPERIMENTAL MODEL AND SUBJECT DETAILS

Human choriocarcinoma JEG-3 cells.—Cells were obtained from the UCSF cell culture facility (but are also available from ATCC) and were grown and maintained in Eagle’s MEM with Earle’s BSS (MEM) supplemented with 10% FBS, 1% NEAA, 1% L-Glutamine, 1% Sodium Pyruvate and 1% Penicillin/Streptomycin. JEG-3 cells are derived from a human male gestational choriocarcinoma.

Larval zebrafish (*Danio rerio*) - wild type AB strain.—Adult zebrafish were raised at the UCSF zebrafish facility at 28°C under a 14/10 hour light /dark cycle in accordance with National Institutes of Health and University of California, San Francisco guidelines. Larval zebrafish (Danio rerio) used for experiments were bred in house and treated in accordance with IACUC regulations. Embryos for experiments were created by matching two females and one male in each breeding tank (three breeding tanks/day for a total of four days), and the resulting embryos pooled for experiments. Assays were run on zebrafish embryos that were at stage 72 to 96 h post fertilization; at these stages there is no way to determine the gender of the embryos because the gonads differentiation starts around 2.5 weeks and it depends on multiple loci/genes and also other epigenetic and environmental factors.

METHOD DETAILS

Nurr1 LBD Constructs—Nurr1 LBD constructs and sequences are described in detail in Table S4. All constructs were subcloned into the pET-DUET-1 Vector (Novagen) within the first multiple cloning site (MCS) and in frame with the N-terminal 6x His tag. The wildtype constructs used for the surface plasmon resonance assays and x-ray crystallography were subcloned into the pET-DUET vector utilizing the BamHI and HindIII restriction sites within the MCS. Note: The N-terminal Ser residue in the crystallography construct (residues Ser-328–598) is an artifact of TEV cleavage (TEV recognition site ENLYFQS, with cleavage between the Q and S) and was not present in the previously reported crystallization construct (Wang et al., 2003). The wildtype construct used for the thermal shift assays was subcloned into the pET-DUET vector using Gibson Cloning. The linearized pET-DUET vector was prepared by PCR amplification, starting at the first multiple cloning site (forward primer: TGCTTAAGTCGAACAGAAAGTAATCG, reverse primer: GGTATATCTCCTTCTTAAAGTTAAAC). The gene inserts (synthesized by Integrated DNA Technologies) including additional 5’ and 3’ Gibson overlap sequences (5’ overlap: GTTTAACTTTAAGAAGGAGATATACC; 3’ overlap: TGCTTAAGTCGAACAGAAAGTAATCG) were then incorporated into the linearized pET-DUET vector using Gibson Assembly (New England BioLabs). The cysteine mutant constructs were prepared using Gibson Cloning as described above (Cys566Thr; gene insert prepared by Integrated DNA technologies) or by custom gene synthesis (Cys465Ala, Cys475Thr, Cys505Thr, Cys534Thr; prepared by GenScript) starting from the wildtype 6xHis Tag – Avi Tag – Nurr1 LBD (363–598) construct (see Table S4).

Protein Expression and Purification

Nurr1 LBD Preparation for Crystallography.: The pET-DUET plasmid harboring the Nurr1 LBD (residues Ser-328–598; Table S4) was transformed into BL21(DE3) (New England BioLabs) or BL21-CodonPlus(DE3)-RIL (Agilent) RILS cells. A single colony was used to inoculate 100 mL of Lysogeny Broth Lennox (LB) medium supplemented with 50 μg/mL ampicillin (as well as 34 μg/mL chloramphenicol in the case of the BL21-CodonPlus strain) and the culture was allowed to grow overnight at 37ºC and 180 rpm. A 10 mL aliquot of the overnight culture was used to inoculate 1 L of LB supplemented with antibiotics as above and the resulting culture was allowed to grow at 37ºC, 180 rpm until reaching an OD_{600} of 0.6 AU, at which time the incubator and cultures were dropped to 16ºC, 180 rpm. Once the culture reached an OD_{600} of 0.8 AU, protein expression was induced by addition of

250 μL of 1M IPTG per 1 L of culture (final concentration 250 μM IPTG) and allowed to proceed overnight (~16 h) at 16ºC and 180 rpm. Cells were then harvested by centrifugation (3500 × g, 20 min), resuspended in ~20 mL of Lysis Buffer per liter of culture using and 18-gauge needle, and lysed by continuous passage at 15,000 psi using a C3 Emulsiflex (Avestin). The soluble Nurr1 LBD was purified from the supernatant using metal affinity chromatography, anion exclusion chromatography, and size exclusion chromatography, as follows. The insoluble fraction was removed by centrifugation (35,000 × g, 30 min). The supernatant was then mixed with 1 mL of TALON resin (Clontech) per liter of culture and allowed to incubate for 2 h at 4ºC with continuous inversion on a rotating wheel. The protein-bound resin was then washed sequentially with 100 mL each of Base Buffer supplemented with 20 mM $MgCl_2$ and 8 mM ATP, Base Buffer supplemented with 100 mM KCl, and Base Buffer supplemented with 25 mM imidazole, prior to elution with 5 mL of Base Buffer supplemented with 300 mM imidazole per liter of culture. Protein was then dialyzed against 1 L of Base Buffer overnight (4ºC, with mixing) in the presence of TEV protease. Cleavage was monitored by SDS-PAGE using a 4–12% Bis-Tris (NuPage). The cleaved protein was then purified by anion exchange chromatography over a MonoQ 10/300GL (GE Healthcare Life Sciences) column using a linear NaCl gradient between Mono Q Buffer A and Mono Q Buffer B (0–50% Buffer B over 10 column volumes). Peaks containing Nurr1 were pooled and then allowed to incubate with TALON resin at 4ºC for 2 h or overnight, with inversion, to remove any residual uncleaved protein. Flow-through from this reverse metal affinity step was then applied to a S75 16/60 SEC column (GE Healthcare Life Sciences) using Base Buffer as the running buffer. The resulting protein was then concentrated and stored at −80ºC for further use. Buffer compositions are as follows: Base Buffer: 50mM HEPES, pH 7.4, 300mM NaCl, 10% Glycerol, 250μM TCEP; Lysis Buffer: Base Buffer + 0.05% Tween 20, 1 cOmplete protease inhibitor tablet (EDTA-free)/50 mL; MonoQ Buffer A: 20mM Tris, pH 7.9, 10% Glycerol, 250μM TCEP; MonoQ Buffer B: MonoQ Buffer A + 1M NaCl.

Nurr1 LBD Preparation for Thermal Shift Assays.: Nurr1 LBD protein was expressed and purified identically to that used for crystallography, except that the TEV cleavage step and reverse immobilized metal affinity chromatography (i.e. incubation with TALON resin) after ion exchange chromatography were omitted. Accordingly, the resulting Nurr1 LBD protein retains an N-terminal 6xHis Tag.

Nurr1 LBD Preparation for Surface Plasmon Resonance Assays.: Nurr1 LBD protein was expressed and purified identically to that used for crystallography, with the following exceptions. The pET-DUET plasmid harboring the Nurr1 LBD containing an N-terminal BirA biotinylation site (“avi-tag”) was co-transformed along with the BirA biotin ligase plasmid (pET21a-BirA; Addgene) into BL21(DE3) bacterial cells (New England BioLabs), and 10 mL of warm 5 mM biotin in 10 mM bicine (pH 8.3) per liter of culture was added along with the IPTG at the time of induction. Purification of the biotinylated Nurr1 LBD proceeded as above, except the TEV cleavage step and anion exchange chromatography steps were omitted (i.e. only the initial metal affinity and size exclusion chromatography were performed). Accordingly, the resulting Nurr1 LBD protein is biotinylated and retains an N-terminal 6xHis Tag.

DHI Preparation—5,6-Dihydroxyindole (Combi-Blocks; QB-2748) and 5,6-dihydroxyindole carboxylic acid (Santa Cruz Biotech; sc-499091) were each prepared as 10 mM and 100 mM stocks in DMSO, aliquoted in small volumes, and stored at −80°C. St ock solutions were prepared rapidly and away from light to minimize oxidation aderivative of the fluorescence signand subsequent polymerization of the compounds. To monitor the stability of these stocks by ^{1}H NMR, 100 mM stocks were also prepared in deuterated DMSO at the same time, stored at −80ºC, and re-examined by NMR annually; no significant changes in the spectra were observed at 12 and 24 months. Once thawed, stocks were never re-used. Investigators planning to carry out experiments with commercially available DHI should verify that the distributor stores their stock under inert gas, away from light, and ideally at < 25ºC. Combi-Blocks confirmed that they store their DHI under argon, in the dark, at 4ºC. NB: Differences in DHI potency observed between cell-free and cellular assays are not unexpected, and are likely a consequence of several unavoidable factors. First, the reaction between DHI and Nurr1 is redox sensitive. The kinetics and thermodynamics of the interaction will likely differ between cell-free (non-reducing) and cellular (highly reducing) environments. Second, DHI/IQ is an unstable molecule that readily polymerizes with itself (and, in cells, with other molecules), reducing the effective concentration of the active ligand over time.

Differential Scanning Fluorimetry Assays—The Nurr1 LBD protein was buffer exchanged from Base Buffer into 25 mM HEPES, 150 mM NaCl, pH 7.4 using a Zeba Spin Desalting Column (ThermoFisher). The DSF assays were carried out in a final volume of 50 μL, comprised of 4 μM protein, 2.5x SYPRO Orange (ThermoFisher/Life Technologies, from 5000x stock), the specified concentration of ligand in DMSO, and reaction buffer comprised of 25 mM HEPES, pH 7.4, 150 mM NaCl (2% final DMSO for each reaction). Samples were allowed to incubate in the dark for 30 min at 25ºC, prior to exposure to thermal gradient. Fluorescence was monitored using the ViiA 7 Real Time PCR System (ThermoFisher) in a 96 well polypropylene plate (Agilent Technologies Cat #410088) using a 2 MicroAmp Optical Adhesive Film, PCR compatible (ThermoFisher Scientific Cat #4311971). The filter used for fluorescent monitoring corresponded to an excitation/emission of 470 ± 15 and 558 ± 11 nm, respectively. The thermal gradient was executed from 25ºC to 95ºC at a rate of 0.05ºC/s. Melting temperatures were determined based on the temperature corresponding to the maximum of derivative of the fluorescence signal (temperature vs dRFU/dT).

Surface Plasmon Resonance Assays—Details for each experiment are summarized in the table below. Data were collected using either a Biacore T100 (GE) or Biacore T200 (GE) instrument at a flow rate of 30 μL/min and at a temperature of 25ºC. The running buffer used in each experiment was either SPR Buffer A: 25mM HEPES, pH 7.4, 150mM NaCl, 0.05% Surfactant P20, and 2% DMSO, or SPR Buffer B: 10mM HEPES, pH 7.4, 150mM NaCl, 0.005% Surfactant P20, 3 mM EDTA, and 2% DMSO (diluted from 10x HBS-EP+; GE Healthcare Life Sciences). The biotinylated Nurr1 LBD was immobilized on a CAP chip (GE Healthcare Life Sciences; product number 28920234). Data collection was performed with one of the following three approaches: (i) no surface regeneration in between injections, (ii) surface regeneration between injections using 6 M guanidium HCl + 0.25 M

NaOH regeneration solution followed by re-immobilization of Nurr1 (as described in the manufacturer's regeneration protocol), or (iii) in single-cycle kinetics mode. DHI, dopamine, and L-DOPA dilutions were carried out starting from DMSO stocks (5 or 10 mM) in DMSO, whereas L-DOPA dilutions were carried out starting from a water stock (5 mM) in water. Analytes dissolved in DMSO were added to 1.02x running buffer without DMSO to yield a final DMSO concentration of 2%. Data processing included double referencing (i.e. reference flow cell and buffer subtracted using a buffer injection of appropriate contact time for the given injection), with solvent correction deemed unnecessary. For the single cycle kinetics approach, DHI was injected at four increasing concentrations (0.62, 1.25, 2.50, 5.00 μM) and responses were normalized to the initial Nurr1 LBD immobilized (summarized below). The surface was regenerated and fresh Nurr1 LBD was immobilized in between single-cycle kinetics experiments.

Figure	Analyte	Nurr1 Immobilized (RU)	Data Collection Mode	Instrument	SPR Buffer
Figure 3A	DHI	wild type (3783)	No Surface Regeneration	T100	A
Figure 3B	DHI	wild type (~1500 /capture)	Surface Regeneration	T100	A
Figure 3C	DHI	wild type (1488), C465A (2515), C475T (1512), C505T (1859), C534T (1582), C566T (1486)	Single Cycle Kinetics	T200	B
Figure S2	DHICA	wild type (3646)	No Surface Regeneration	T100	A
Figure S2	Dopamine	wild type (1761)	No Surface Regeneration	T200	B
Figure S2	L-DOPA	wild type (1635)	No Surface Regeneration	T200	B

Determining Ligand Stoichiometry.: The theoretical Rmax for DHI binding to the primary site (n = 1), and additionally to the secondary site (n = 2), in the Nurr1 LBD was calculated using the molecular weights of DHI (analyte) and the Nurr1 LBD (ligand), and the amount (RU) of immobilized Nurr1 captured to the chip (as described in the Biacore Handbook available online). The general equation is as follows:

Rmax (RU) = (analyte MW / ligand MW) × (immobilized ligand level in RU) × analyte stoichiometry

For our assays (see Figure 3B), the theoretical Rmax for one and two molecules of DHI bound per Nurr1 LBD was calculated as follows:

(n = 1 DHI/IQ bound) Rmax = (A / B) × (C × 1)

(n = 2 DHI/IQ bound) Rmax = (A / B) × (C × 2)

where A = 150 Da for DHI; B = 30632 Da and 30630 Da for the wildtype and cysteine point mutant Nurr1 LBDs, respectively; C = RU for Nurr1 immobilized in each experiment (see above).

Crystallography of the Nurr1 LBD

Crystallization.: The Nurr1 LBD was buffer exchanged into 150 mM NaCl, 25 mM HEPES, pH 7.4 using a 7 kD cutoff Zeba Desalting Column. DHI was then added to a final concentration of 200 μM (2% DMSO) from a 10 mM stock to a protein solution of 228 μM. The reaction was allowed to proceed on ice for 15 min before excess DHI and DMSO were removed via buffer exchange as described above. This labeling procedure was then repeated for a second time. Crystals were then prepared using a custom screen surrounding the previously reported crystallization condition (18% PEG3350, 200 mM KBr, 100 mM HEPES, pH 6.5)(Wang et al., 2003), with a pH range of 6.5–8.0 generated by mixing various volumes of 100 mM HEPES at pH 6.5 and 8.0. Crystals grew in a 96-well hanging drop format (1 drop per well) as 500 nL drops consisting of a 1:1 ratio of protein to condition with initial protein concentrations ranging from 4–7 mg/mL. Crystals were transferred briefly into the crystallization condition supplemented with 20% ethylene glycol to serve as a cryoprotectant prior to plunging into liquid nitrogen. The best diffracting crystal described herein was ~200 μm × 50 μm × 50 μm in size and cyroprotected 30 days after the initial drops were set.

Data Collection.: Data was collected as the Advanced Light Source, Beamline 8.3.1 at an energy of 11111eV on a ADSC Quantum 315r S/N 926 detector under a stream of liquid nitrogen.

Structure Determination.: Data were integrated and scaled using XDS (Kabsch, 2010). Although these crystals grew isomorphous to the deposited apo structure (PDB: 1OVL), crystals can reportedly grow as either the $P3_1$ or $P3_12_1$ space group (Wang et al., 2003). Exhaustive attempts at reaching an initial molecular replacement solution using the previously deposited apo Nurr1 LBD structure were unsuccessful, regardless of which space group was chosen for processing. We were initially able to refine this model using phenix.refine (Afonine et al., 2012) using the hexamer from 1OVL after applying the appropriate $P3_1$ reindexing operator (-h,-k,l or - k,-h,-l). However, the Rwork-Rfree gap was ~10% after many rounds of refinement (and could not be closed), indicating that the higher symmetry $P3_12_1$ might be the appropriate space group. We utilized Zanuda (Lebedev and Isupov, 2014) to help explore the higher symmetry $P3_12_1$ as a potential space group with a trimer of Nurr1 monomers as the asymmetric unit. Zanuda successfully identified one potential trimer that could serve as an initial model for refinement. The data were then merged as $P3_12_1$ using this trimer (chains A, B, and C of PDB: 1OVL) as a reference with the program *pointless* (Evans, 2011) followed by scaling with *aimless* (Evans and Murshudov, 2013). Iterative rounds of phenix.refine and model building with COOT (Emsley et al., 2010) were able to refine the model to within reasonable structure validation metrics. Chains A, B, and C of PDB: 1OVL were also used as a reference model for refinement. After several rounds of refinement and rebuilding, the Cys-IQ C2-adduct was introduced at Cys566 for chains A, B, and C using computational modeling as described below. TLS refinement and target-weight optimization for both XYZ and ADP restraints were performed. Occupancies were refined for the Cys-IQ C2-adducts (DHI/IQ atoms only, not Cys566 atoms) to allow for only partial adduct formation. Finally, phenix.polder was used to calculate difference maps for the adduct (Liebschner et al., 2017).

Initial Model Building of IQ Covalently Bound to Cys566.: A partially refined structure without the Cys566-IQ adduct built in was used as a starting structure for computational modeling. The unnatural amino acid residue Cys566-IQ (N-methylated and C-acetylated) linked to IQ at the C2 atom was built within Maestro within the Schrodinger Suite. Hetgrp_ffgen (Schrodinger utilities) was then used to generate parameters for this adduct. The program PLOP (Jacobson et al., 2004) was then used to perform covalent docking for this cysteine adduct using 500,000 conformations followed by energy minimization of the introduced adduct. This model was then further refined with phenix.refine using a ligand restraint file for the Cys-IQ adduct (described below).

Ligand Restraint Generation.: The Cys566-IQ unnatural amino acid was exported from Maestro in SMILES format and opened in JLigand. Atom names were manually modified to match the pdb atoms from the model generated using PLOP. This structure was saved as a cif file and used as a template for phenix.elbow (Moriarty et al., 2009) ligand restraint generation using AM1 optimization.

Positional Scanning Simulations—To explore the positional preference for thiolate attack, potential energy surfaces for the catechol and the quinone forms of DHI were scanned. All quantum mechanics calculations were carried out by using the Gaussian 09 software (Frisch et al., 2016). Geometries were optimized at the B3LYP/6–311+G(d) level.

Luciferase Reporter Assays—Human choriocarcinoma JEG-3 cells were maintained in Eagle's MEM with Earle's BSS (MEM) supplemented with 10% FBS, 1% NEAA, 1% L-Glutamine, 1% Sodium Pyruvate and 1% Penicillin/Streptomycin. For transfection, cells were seeded in 96-well plate in antibiotic free medium one day before transfection. Transfections were carried out with Lipofectamine 2000 (Invitrogen) according to manufacturer's protocol. Lipofectamine/DNA complexes were prepared in Opti-Mem medium and incubated with cells overnight. The Nurr1 LBD fragment was subcloned into pM plasmid (Clontech) containing GAL4 DNA binding domain. The reporter plasmid, pGL4.35 (luc2P/9XGAL4 UAS/Hygro) Vector (Promega), contains 9 repeats of GAL4 UAS (Upstream Activator Sequence), which drives transcription of the luciferase reporter gene luc2P in response to binding of Gal4 DNA binding domain fused protein. The pRL-TK (Promega) plasmid expressing renilla luciferase was used as an internal control. The amounts of pM-Nurr1-LBD, pGL4.35 and pRL-TK were 50 ng, 50 ng and 5 ng per well respectively. Six hours before luciferase measurement, different doses of DHI were added and incubated. Cells from each well were lysed with 100 μl Passive Lysis Buffer (Promega). The luciferase activities of firefly and renilla were measured using Dual-Luciferase® Reporter Assay System (Promega) according to manufacturer's protocol. GraphPad Prism 7 software was used for statistical analysis. The results were expressed as average of firefly/renilla luciferase activity ± SD (n = 4).

Target Gene Transcription Assays

DHI Administration.: Larval zebrafish (Danio rerio) used for experiments were bred in house and treated in accordance with IACUC regulations. Fifty zebrafish larvae per concentration per experiment, for a total of 200 larvae per concentration (replicates = 4)

were treated in a 10 cm Petri dishes at 72 h post fertilization (hpf) with DHI diluted (100 mM stock) into 40 mL of blue egg water (lab stock) to reach final concentrations of 10 and 100 μM (0.2% DMSO). Control larvae were exposed to an equivalent amount of DMSO (0.2%). Samples were collected for further analysis 6 and 24 h post treatment.

RNA Isolation and Transcript Quantification.: Total RNA was extracted from zebrafish larvae (collection post-treatment at 78 hpf after 6 h DHI exposure and 96 hpf after 24 h DHI exposure) using TRIzol reagent (Invitrogen) by homogenization and purified using RNeasy Mini Kit (Qiagen). The cDNA was then synthesized from 160 ng of purified RNA using qScript cDNA SuperMix (Quanta Biosciences) and used as template. The qPCR was performed using Applied Biosystems SYBR Green PCR Master Mix and the ABI7900HT machine. The forward and reverse primers (Table S5) were designed using NCBI/primer-BLAST software with exon-exon junction parameters and *Danio rerio* RefSeq for off targets. The elongation factor 1 alpha (*elf1α)* gene was used as internal housekeeping gene to determine the relative mRNA expression. The *elf1α* primers were used as standard control (McCurley and Callard, 2008) to generate Ct values. Transcript levels for target genes were normalized to the housekeeping gene *elf1a* and fold change was compared to gene expression levels from DMSO-treated larvae. GraphPad Prism 7 software was used for statistical analysis. Unpaired Student t-test was applied for DMSO ct *vs* 10 μM and 100 μM DHI. Results are from four independent experiments. Relative average expression ± SEM; *p < 0.05, **p < 0.01, ***p < 0.001 by Student's t-test in comparison expression with 0 μM compound (DMSO only). Significant results (P values) were observed for the following conditions: 6 h 100 μM DHI treatment (*vmat2* = 0.019; *dat* = 0.015) and 24 h 100 μM DHI treatment (*th* = 0.030 and *vmat2* = 0.00008).

QUANTIFICATION AND STATISCAL ANALYSIS

The Unpaired Student's t-test or One-way Analysis of Variance (ANOVA) were used to determine statistical significance using GraphPad Prism 7 software. Statistical details for of experiments can be found in the individual Figure Legend and Method Details section. Data are considered significantly different when P ≤ 0.05*; P ≤ 0.01**; P ≤ 0.001***; P ≤ 0.0001****. Differential scanning fluorimetry assay plots of the change in melting temperature (T_M) as a function of the drug (DHI or DHICA) concentration are expressed as the average T_M ± SD, derived from three independent experiments. Luciferase reporter assay results are expressed as the average of the firefly/renilla luciferase signal ± SD, derived from four independent experiments. Zebrafish target gene transcription assay results are expressed the average of gene transcript level ± SEM, derived from four independent experiments.

Supplementary Material

Refer to Web version on PubMed Central for supplementary material.

ACKNOWLEDGMENTS

This work was supported by grants from the Roger's Family Foundation, the CTSI, the MAKK Seed Fund, the NIH (R01 NS108404–01), and the Program for Breakthrough Biomedical Research that is partially funded by the Sandler Foundation. We thank Joseph Wagner for helpful discussions. Beamline 8.3.1 at the Advanced Light Source is operated by the University of California Office of the President, Multicampus Research Programs and Initiatives

grant MR-15–328599 the National Institutes of Health (R01 GM124149 and P30 GM124169), Plexxikon Inc. and the Integrated Diffraction Analysis Technologies program of the US Department of Energy Office of Biological and Environmental Research. The Advanced Light Source (Berkeley, CA) is a national user facility operated by Lawrence Berkeley National Laboratory on behalf of the US Department of Energy under contract number DE-AC02–05CH11231, Office of Basic Energy Sciences.

REFERENCES

Aarnisalo P, Kim CH, Lee JW, and Perlmann T (2002). Defining requirements for heterodimerization between the retinoid × receptor and the orphan nuclear receptor Nurr1. J. Biol. Chem 277, 35118–35123. [PubMed: 12130634]

Afonine PV, Grosse-Kunstleve RW, Echols N, Headd JJ, Moriarty NW, Mustyakimov M, Terwilliger TC, Urzhumtsev A, Zwart PH, and Adams PD (2012). Towards automated crystallographic structure refinement with phenix.refine. Acta Crystallogr. D Biol. Crystallogr 68, 352–367.

Alavian KN, Jeddi S, Naghipour SI, Nabili P, Licznerski P, and Tierney TS (2014). The lifelong maintenance of mesencephalic dopaminergic neurons by Nurr1 and engrailed. J. Biomed. Sci 21, 27. [PubMed: 24685177]

Alter SP, Lenzi GM, Bernstein AI, and Miller GW (2013). Vesicular integrity in Parkinson's disease. Curr. Neurol. Neurosci. Rep 13, 362. [PubMed: 23690026]

Armarego WL, and Waring P (1983). Inhibition of human brain dihydropteridine reductase [E.C.1.6.99.10] by the oxidation products of catecholamines, the aminochromes. Biochem. Biophys. Res. Commun 113, 895–899. [PubMed: 6870900]

Belluzzi E, Bisaglia M, Lazzarini E, Tabares LC, Beltramini M, and Bubacco L (2012). Human SOD2 modification by dopamine quinones affects enzymatic activity by promoting its aggregation: possible implications for Parkinson's disease. PLoS One 7, e38026. [PubMed: 22723845]

Bisaglia M, Mammi S, and Bubacco L (2007). Kinetic and structural analysis of the early oxidation products of dopamine: analysis of the interactions with alpha-synuclein. J. Biol. Chem 282, 15597–15605. [PubMed: 17395592]

Blesa J, Trigo-Damas I, Quiroga-Varela A, and Jackson-Lewis VR (2015). Oxidative stress and Parkinson's disease. Front. Neuroanat 9, 91. [PubMed: 26217195]

Blin M, Norton W, Bally-Cuif L, and Vernier P (2008). NR4A2 controls the differentiation of selective dopaminergic nuclei in the zebrafish brain. Mol. Cell. Neurosci 39, 592–604. [PubMed: 18822380]

Brighina L, Riva C, Bertola F, Saracchi E, Fermi S, Goldwurm S, and Ferrarese C (2013). Analysis of vesicular monoamine transporter 2 polymorphisms in Parkinson's disease. Neurobiol. Aging 34, 1712 e1719–1713.

Burbulla LF, Song P, Mazzulli JR, Zampese E, Wong YC, Jeon S, Santos DP, Blanz J, Obermaier CD, Strojny C, et al. (2017). Dopamine oxidation mediates mitochondrial and lysosomal dysfunction in Parkinson's disease. Science 357, 1255–1261. [PubMed: 28882997]

Castro DS, Arvidsson M, Bondesson Bolin M., and Perlmann T (1999). Activity of the Nurr1 carboxyl-terminal domain depends on cell type and integrity of the activation function 2. J. Biol. Chem 274, 37483–37490. [PubMed: 10601324]

Caudle WM, Richardson JR, Wang MZ, Taylor TN, Guillot TS, McCormack AL, Colebrooke RE, Di Monte DA, Emson PC, and Miller GW (2007). Reduced vesicular storage of dopamine causes progressive nigrostriatal neurodegeneration. J. Neurosci 27, 8138–8148. [PubMed: 17652604]

Chen L, Ding Y, Cagniard B, Van Laar AD, Mortimer A, Chi W, Hastings TG, Kang UJ, and Zhuang X (2008). Unregulated cytosolic dopamine causes neurodegeneration associated with oxidative stress in mice. J. Neurosci 28, 425–433. [PubMed: 18184785]

Chu Y, Le W, Kompoliti K, Jankovic J, Mufson EJ, and Kordower JH (2006). Nurr1 in Parkinson's disease and related disorders. J. Comp. Neurol 494, 495–514. [PubMed: 16320253]

Codina A, Benoit G, Gooch JT, Neuhaus D, Perlmann T, and Schwabe JW (2004). Identification of a novel co-regulator interaction surface on the ligand binding domain of Nurr1 using NMR footprinting. J. Biol. Chem 279, 53338–53345. [PubMed: 15456745]

d'Ischia M, Napolitano A, and Pezzella A (2011). 5,6-Dihydroxyindole Chemistry: Unexplored Opportunities Beyond Eumelanin. Eur. J. Org. Chem, 5501–5516.

d'Ischia M, Napolitano A, Pezzella A, Land EJ, Ramsden CA, and Riley PA (2005). 5,6-dihydroxyrindoles and Indole-5,6-diones. Advances in Heterocyclic Chemistry, Vol 89 89, 1–63.

d'Ischia M, Napolitano A, and Prota G (1987). Sulphydryl compounds in melanogenesis. Part I. Reaction of cysteine and glutathione with 5,6-dihydroxyindole. Tetrahedron 43, 5351–5356.

de Lau LM, and Breteler MM (2006). Epidemiology of Parkinson's disease. Lancet Neurol 5, 525–535. [PubMed: 16713924]

de Vera IM, Giri PK, Munoz-Tello P, Brust R, Fuhrmann J, Matta-Camacho E, Shang J, Campbell S, Wilson HD, Granados J, et al. (2016). Identification of a Binding Site for Unsaturated Fatty Acids in the Orphan Nuclear Receptor Nurr1. ACS Chem. Biol 11, 1795–1799. [PubMed: 27128111]

Decressac M, Volakakis N, Bjorklund A, and Perlmann T (2013). NURR1 in Parkinson disease--from pathogenesis to therapeutic potential. Nat. Rev. Neurol 9, 629–636. [PubMed: 24126627]

Dischia M, Napolitano A, and Prota G (1987). Sulfhydryl Compounds in Melanogenesis .1. Reaction of Cysteine and Glutathione with 5,6-Dihydroxyindoles. Tetrahedron 43, 5351–5356.

Dong J, Li S, Mo JL, Cai HB, and Le WD (2016). Nurr1-Based Therapies for Parkinson's Disease. CNS Neurosci. Ther 22, 351–359. [PubMed: 27012974]

Eisenhofer G, Kopin IJ, and Goldstein DS (2004). Leaky catecholamine stores: undue waste or a stress response coping mechanism? Ann. N. Y. Acad. Sci 1018, 224–230. [PubMed: 15240373]

Emsley P, Lohkamp B, Scott WG, and Cowtan K (2010). Features and development of Coot. Acta Crystallogr. D Biol. Crystallogr 66, 486–501. [PubMed: 20383002]

Evans PR (2011). An introduction to data reduction: space-group determination, scaling and intensity statistics. Acta Crystallogr. D Biol. Crystallogr 67, 282–292. [PubMed: 21460446]

Evans PR, and Murshudov GN (2013). How good are my data and what is the resolution? Acta Crystallogr. D Biol. Crystallogr 69, 1204–1214. [PubMed: 23793146]

Fedorow H, Halliday GM, Rickert CH, Gerlach M, Riederer P, and Double KL (2006). Evidence for specific phases in the development of human neuromelanin. Neurobiol. Aging 27, 506–512. [PubMed: 15916835]

Frisch MJ, Trucks GW, Schlegel HB, Scuseria GE, Robb MA, Cheeseman JR, Scalmani G, Barone V, Petersson GA, Nakatsuji H, et al. (2016). Gaussian 09, Revision E.01

Gallastegui N, Mackinnon JA, Fletterick RJ, and Estebanez-Perpina E (2015). Advances in our structural understanding of orphan nuclear receptors. Trends Biochem. Sci 40, 25–35. [PubMed: 25499868]

Galleguillos D, Fuentealba JA, Gomez LM, Saver M, Gomez A, Nash K, Burger C, Gysling K, and Andres ME (2010). Nurr1 regulates RET expression in dopamine neurons of adult rat midbrain. J. Neurochem 114, 1158–1167. [PubMed: 20533997]

Gallivan JP, and Dougherty DA (1999). Cation-pi interactions in structural biology. Proc. Natl. Acad. Sci. U. S. A 96, 9459–9464. [PubMed: 10449714]

Garcia-Yague AJ, Rada P, Rojo AI, Lastres-Becker I, and Cuadrado A (2013). Nuclear import and export signals control the subcellular localization of Nurr1 protein in response to oxidative stress. J. Biol. Chem 288, 5506–5517. [PubMed: 23283970]

Girotto S, Sturlese M, Bellanda M, Tessari I, Cappellini R, Bisaglia M, Bubacco L, and Mammi S (2012). Dopamine-derived quinones affect the structure of the redox sensor DJ-1 through modifications at Cys-106 and Cys-53. J. Biol. Chem 287, 18738–18749. [PubMed: 22431735]

Glatt CE, Wahner AD, White DJ, Ruiz-Linares A, and Ritz B (2006). Gain-of-function haplotypes in the vesicular monoamine transporter promoter are protective for Parkinson disease in women. Hum. Mol. Genet 15, 299–305. [PubMed: 16339215]

Grimes DA, Han F, Panisset M, Racacho L, Xiao F, Zou R, Westaff K, and Bulman DE (2006). Translated mutation in the Nurr1 gene as a cause for Parkinson's disease. Mov. Disord 21, 906–909. [PubMed: 16532445]

Gronemeyer H, Gustafsson JA, and Laudet V (2004). Principles for modulation of the nuclear receptor superfamily. Nat Rev Drug Discov 3, 950–964. [PubMed: 15520817]

Guillot TS, and Miller GW (2009). Protective actions of the vesicular monoamine transporter 2 (VMAT2) in monoaminergic neurons. Mol. Neurobiol 39, 149–170. [PubMed: 19259829]

Guillot TS, Shepherd KR, Richardson JR, Wang MZ, Li Y, Emson PC, and Miller GW (2008). Reduced vesicular storage of dopamine exacerbates methamphetamine-induced neurodegeneration and astrogliosis. J. Neurochem 106, 2205–2217. [PubMed: 18643795]

Hastings TG (2009). The role of dopamine oxidation in mitochondrial dysfunction: implications for Parkinson's disease. J. Bioenerg. Biomembr 41, 469–472. [PubMed: 19967436]

Hauser DN, and Hastings TG (2013). Mitochondrial dysfunction and oxidative stress in Parkinson's disease and monogenic parkinsonism. Neurobiol. Dis 51, 35–42. [PubMed: 23064436]

Hermanson E, Joseph B, Castro D, Lindqvist E, Aarnisalo P, Wallen A, Benoit G, Hengerer B, Olson L, and Perlmann T (2003). Nurr1 regulates dopamine synthesis and storage in MN9D dopamine cells. Exp. Cell Res 288, 324–334. [PubMed: 12915123]

Huang P, Chandra V, and Rastinejad F (2010). Structural overview of the nuclear receptor superfamily: insights into physiology and therapeutics. Annu. Rev. Physiol 72, 247–272. [PubMed: 20148675]

Hwang O (2013). Role of oxidative stress in Parkinson's disease. Exp. Neurobiol 22, 11–17. [PubMed: 23585717]

Iwawaki T, Kohno K, and Kobayashi K (2000). Identification of a potential nurr1 response element that activates the tyrosine hydroxylase gene promoter in cultured cells. Biochem. Biophys. Res. Commun 274, 590–595. [PubMed: 10924322]

Jacobson MP, Pincus DL, Rapp CS, Day TJ, Honig B, Shaw DE, and Friesner RA (2004). A hierarchical approach to all-atom protein loop prediction. Proteins 55, 351–367. [PubMed: 15048827]

Janezic S, Threlfell S, Dodson PD, Dowie MJ, Taylor TN, Potgieter D, Parkkinen L, Senior SL, Anwar S, Ryan B, et al. (2013). Deficits in dopaminergic transmission precede neuron loss and dysfunction in a new Parkinson model. Proc. Natl. Acad. Sci. U. S. A 110, E4016–4025. [PubMed: 24082145]

Jankovic J, Chen S, and Le WD (2005). The role of Nurr1 in the development of dopaminergic neurons and Parkinson's disease. Prog. Neurobiol 77, 128–138. [PubMed: 16243425]

Jenner P (2003). Oxidative stress in Parkinson's disease. Ann. Neurol 53 Suppl 3, S26–36; discussion S36–28. [PubMed: 12666096]

Jiang C, Wan X, He Y, Pan T, Jankovic J, and Le W (2005). Age-dependent dopaminergic dysfunction in Nurr1 knockout mice. Exp. Neurol 191, 154–162. [PubMed: 15589522]

Johnson MM, Michelhaugh SK, Bouhamdan M, Schmidt CJ, and Bannon MJ (2011). The Transcription Factor NURR1 Exerts Concentration-Dependent Effects on Target Genes Mediating Distinct Biological Processes. Front. Neurosci 5, 135. [PubMed: 22194714]

Kabsch W (2010). Integration, scaling, space-group assignment and post-refinement. Acta Crystallogr. D Biol. Crystallogr 66, 133–144. [PubMed: 20124693]

Kadkhodaei B, Alvarsson A, Schintu N, Ramskold D, Volakakis N, Joodmardi E, Yoshitake T, Kehr J, Decressac M, Bjorklund A, et al. (2013). Transcription factor Nurr1 maintains fiber integrity and nuclear-encoded mitochondrial gene expression in dopamine neurons. Proc. Natl. Acad. Sci. U. S. A 110, 2360–2365. [PubMed: 23341612]

Kadkhodaei B, Ito T, Joodmardi E, Mattsson B, Rouillard C, Carta M, Muramatsu S, Sumi-Ichinose C, Nomura T, Metzger D, et al. (2009). Nurr1 is required for maintenance of maturing and adult midbrain dopamine neurons. J. Neurosci 29, 15923–15932. [PubMed: 20016108]

Kim CH, Han BS, Moon J, Kim DJ, Shin J, Rajan S, Nguyen QT, Sohn M, Kim WG, Han M, et al. (2015). Nuclear receptor Nurr1 agonists enhance its dual functions and improve behavioral deficits in an animal model of Parkinson's disease. Proc. Natl. Acad. Sci. U. S. A 112, 8756–8761. [PubMed: 26124091]

Kim KS, Kim CH, Hwang DY, Seo H, Chung S, Hong SJ, Lim JK, Anderson T, and Isacson O (2003). Orphan nuclear receptor Nurr1 directly transactivates the promoter activity of the tyrosine hydroxylase gene in a cell-specific manner. J. Neurochem 85, 622–634. [PubMed: 12694388]

Krasnova IN, and Cadet JL (2009). Methamphetamine toxicity and messengers of death. Brain Res Rev 60, 379–407. [PubMed: 19328213]

Kuhn DM, Arthur RE Jr., Thomas DM, and Elferink LA (1999). Tyrosine hydroxylase is inactivated by catechol-quinones and converted to a redox-cycling quinoprotein: possible relevance to Parkinson's disease. J. Neurochem 73, 1309–1317. [PubMed: 10461926]

Kumar R, and McEwan IJ (2012). Allosteric modulators of steroid hormone receptors: structural dynamics and gene regulation. Endocr. Rev 33, 271–299. [PubMed: 22433123]

LaVoie MJ, Ostaszewski BL, Weihofen A, Schlossmacher MG, and Selkoe DJ (2005). Dopamine covalently modifies and functionally inactivates parkin. Nat. Med 11, 1214–1221. [PubMed: 16227987]

Le W, Pan T, Huang M, Xu P, Xie W, Zhu W, Zhang X, Deng H, and Jankovic J (2008). Decreased NURR1 gene expression in patients with Parkinson's disease. J. Neurol. Sci 273, 29–33. [PubMed: 18684475]

Le WD, Xu P, Jankovic J, Jiang H, Appel SH, Smith RG, and Vassilatis DK (2003). Mutations in NR4A2 associated with familial Parkinson disease. Nat. Genet 33, 85–89. [PubMed: 12496759]

Lebedev AA, and Isupov MN (2014). Space-group and origin ambiguity in macromolecular structures with pseudo-symmetry and its treatment with the program Zanuda. Acta Crystallogr. D Biol. Crystallogr 70, 2430–2443. [PubMed: 25195756]

Lee G, Elwood F, McNally J, Weiszmann J, Lindstrom M, Amaral K, Nakamura M, Miao S, Cao P, Learned RM, et al. (2002). T0070907, a selective ligand for peroxisome proliferator-activated receptor gamma, functions as an antagonist of biochemical and cellular activities. J. Biol. Chem 277, 19649–19657. [PubMed: 11877444]

Liebschner D, Afonine PV, Moriarty NW, Poon BK, Sobolev OV, Terwilliger TC, and Adams PD (2017). Polder maps: improving OMIT maps by excluding bulk solvent. Acta Crystallogr D Struct Biol 73, 148–157. [PubMed: 28177311]

Lohr KM, Bernstein AI, Stout KA, Dunn AR, Lazo CR, Alter SP, Wang M, Li Y, Fan X, Hess EJ, et al. (2014). Increased vesicular monoamine transporter enhances dopamine release and opposes Parkinson disease-related neurodegeneration in vivo. Proc. Natl. Acad. Sci. U. S. A 111, 9977–9982. [PubMed: 24979780]

Lotharius J, and Brundin P (2002). Pathogenesis of Parkinson's disease: dopamine, vesicles and alpha-synuclein. Nat. Rev. Neurosci 3, 932–942. [PubMed: 12461550]

Luo Y (2012). The function and mechanisms of Nurr1 action in midbrain dopaminergic neurons, from development and maintenance to survival. Int. Rev. Neurobiol 102, 1–22. [PubMed: 22748824]

Maira M, Martens C, Philips A, and Drouin J (1999). Heterodimerization between members of the Nur subfamily of orphan nuclear receptors as a novel mechanism for gene activation. Mol. Cell. Biol 19, 7549–7557. [PubMed: 10523643]

Mason HS, and Peterson EW (1965). Melanoproteins. I. Reactions between enzyme-generated quinones and amino acids. Biochim. Biophys. Acta 111, 134–146. [PubMed: 5893781]

McCurley AT, and Callard GV (2008). Characterization of housekeeping genes in zebrafish: male-female differences and effects of tissue type, developmental stage and chemical treatment. BMC Mol. Biol 9, 102. [PubMed: 19014500]

McFarland K, Spalding TA, Hubbard D, Ma JN, Olsson R, and Burstein ES (2013). Low dose bexarotene treatment rescues dopamine neurons and restores behavioral function in models of Parkinson's disease. ACS Chem. Neurosci 4, 1430–1438. [PubMed: 24117438]

Meiser J, Weindl D, and Hiller K (2013). Complexity of dopamine metabolism. Cell Commun Signal 11, 34. [PubMed: 23683503]

Montarolo F, Perga S, Martire S, Navone DN, Marchet A, Leotta D, and Bertolotto A (2016). Altered NR4A Subfamily Gene Expression Level in Peripheral Blood of Parkinson's and Alzheimer's Disease Patients. Neurotox. Res 30, 338–344. [PubMed: 27159982]

Moran LB, Croisier E, Duke DC, Kalaitzakis ME, Roncaroli F, Deprez M, Dexter DT, Pearce RK, and Graeber MB (2007). Analysis of alpha-synuclein, dopamine and parkin pathways in neuropathologically confirmed parkinsonian nigra. Acta Neuropathol 113, 253–263. [PubMed: 17203291]

Moriarty NW, Grosse-Kunstleve RW, and Adams PD (2009). electronic Ligand Builder and Optimization Workbench (eLBOW): a tool for ligand coordinate and restraint generation. Acta Crystallogr. D Biol. Crystallogr 65, 1074–1080. [PubMed: 19770504]

Mosharov EV, Gong LW, Khanna B, Sulzer D, and Lindau M (2003). Intracellular patch electrochemistry: regulation of cytosolic catecholamines in chromaffin cells. J. Neurosci 23, 5835–5845. [PubMed: 12843288]

Mosharov EV, Staal RG, Bove J, Prou D, Hananiya A, Markov D, Poulsen N, Larsen KE, Moore CM, Troyer MD, et al. (2006). Alpha-synuclein overexpression increases cytosolic catecholamine concentration. J. Neurosci 26, 9304–9311. [PubMed: 16957086]

Niesen FH, Berglund H, and Vedadi M (2007). The use of differential scanning fluorimetry to detect ligand interactions that promote protein stability. Nat. Protoc 2, 2212–2221. [PubMed: 17853878]

Olefirowicz TM, and Ewing AG (1990). Dopamine concentration in the cytoplasmic compartment of single neurons determined by capillary electrophoresis. J. Neurosci. Methods 34, 11–15. [PubMed: 2259233]

Omiatek DM, Bressler AJ, Cans AS, Andrews AM, Heien ML, and Ewing AG (2013). The real catecholamine content of secretory vesicles in the CNS revealed by electrochemical cytometry. Sci. Rep 3, 1447. [PubMed: 23486177]

Paulsen RF, Granas K, Johnsen H, Rolseth V, and Sterri S (1995). Three related brain nuclear receptors, NGFI-B, Nurr1, and NOR-1, as transcriptional activators. J. Mol. Neurosci 6, 249–255. [PubMed: 8860236]

Perez E, Bourguet W, Gronemeyer H, and de Lera AR (2012). Modulation of RXR function through ligand design. Biochim. Biophys. Acta 1821, 57–69. [PubMed: 21515403]

Perlmann T, and Jansson L (1995). A novel pathway for vitamin A signaling mediated by RXR heterodimerization with NGFI-B and NURR1. Genes Dev 9, 769–782. [PubMed: 7705655]

Philips A, Lesage S, Gingras R, Maira MH, Gauthier Y, Hugo P, and Drouin J (1997). Novel dimeric Nur77 signaling mechanism in endocrine and lymphoid cells. Mol. Cell. Biol 17, 5946–5951. [PubMed: 9315652]

Pifl C, Rajput A, Reither H, Blesa J, Cavada C, Obeso JA, Rajput AH, and Hornykiewicz O (2014). Is Parkinson's disease a vesicular dopamine storage disorder? Evidence from a study in isolated synaptic vesicles of human and nonhuman primate striatum. J. Neurosci 34, 8210–8218. [PubMed: 24920625]

Poppe L, Harvey TS, Mohr C, Zondlo J, Tegley CM, Nuanmanee O, and Cheetham J (2007). Discovery of ligands for Nurr1 by combined use of NMR screening with different isotopic and spin-labeling strategies. J Biomol Screen 12, 301–311. [PubMed: 17438066]

Reese JC, Wooge CH, and Katzenellenbogen BS (1992). Identification of two cysteines closely positioned in the ligand-binding pocket of the human estrogen receptor: roles in ligand binding and transcriptional activation. Mol. Endocrinol 6, 2160–2166. [PubMed: 1491695]

Sacchetti P, Mitchell TR, Granneman JG, and Bannon MJ (2001). Nurr1 enhances transcription of the human dopamine transporter gene through a novel mechanism. J. Neurochem 76, 1565–1572. [PubMed: 11238740]

Saijo K, Winner B, Carson CT, Collier JG, Boyer L, Rosenfeld MG, Gage FH, and Glass CK (2009). A Nurr1/CoREST pathway in microglia and astrocytes protects dopaminergic neurons from inflammation-induced death. Cell 137, 47–59. [PubMed: 19345186]

Sakurada K, Ohshima-Sakurada M, Palmer TD, and Gage FH (1999). Nurr1, an orphan nuclear receptor, is a transcriptional activator of endogenous tyrosine hydroxylase in neural progenitor cells derived from the adult brain. Development 126, 4017–4026. [PubMed: 10457011]

Samii A, Nutt JG, and Ransom BR (2004). Parkinson's disease. Lancet 363, 1783–1793. [PubMed: 15172778]

Segura-Aguilar J, Paris I, Munoz P, Ferrari E, Zecca L, and Zucca FA (2014). Protective and toxic roles of dopamine in Parkinson's disease. J. Neurochem 129, 898–915. [PubMed: 24548101]

Smith GA, Rocha EM, Rooney T, Barneoud P, McLean JR, Beagan J, Osborn T, Coimbra M, Luo Y, Hallett PJ, et al. (2015). A Nurr1 agonist causes neuroprotection in a Parkinson's disease lesion model primed with the toll-like receptor 3 dsRNA inflammatory stimulant poly(I:C). PLoS One 10, e0121072. [PubMed: 25815475]

Spathis AD, Asvos X, Ziavra D, Karampelas T, Topouzis S, Cournia Z, Qing X, Alexakos P, Smits LM, Dalla C, et al. (2017). Nurr1:RXRalpha heterodimer activation as monotherapy for Parkinson's disease. Proc. Natl. Acad. Sci. U. S. A 114, 3999–4004. [PubMed: 28348207]

Sulzer D, Bogulavsky J, Larsen KE, Behr G, Karatekin E, Kleinman MH, Turro N, Krantz D, Edwards RH, Greene LA, et al. (2000). Neuromelanin biosynthesis is driven by excess cytosolic

catecholamines not accumulated by synaptic vesicles. Proc. Natl. Acad. Sci. U. S. A 97, 11869–11874. [PubMed: 11050221]

Sulzer D, and Zecca L (2000). Intraneuronal dopamine-quinone synthesis: a review. Neurotox. Res 1, 181–195. [PubMed: 12835101]

Ulusoy A, Bjorklund T, Buck K, and Kirik D (2012). Dysregulated dopamine storage increases the vulnerability to alpha-synuclein in nigral neurons. Neurobiol. Dis 47, 367–377. [PubMed: 22659302]

Volakakis N, Malewicz M, Kadkhodai B, Perlmann T, and Benoit G (2006). Characterization of the Nurr1 ligand-binding domain co-activator interaction surface. J. Mol. Endocrinol 37, 317–326. [PubMed: 17032747]

Volakakis N, Tiklova K, Decressac M, Papathanou M, Mattsson B, Gillberg L, Nobre A, Bjorklund A, and Perlmann T (2015). Nurr1 and Retinoid × Receptor Ligands Stimulate Ret Signaling in Dopamine Neurons and Can Alleviate alpha-Synuclein Disrupted Gene Expression. J. Neurosci 35, 14370–14385. [PubMed: 26490873]

Volpicelli F, Caiazzo M, Greco D, Consales C, Leone L, Perrone-Capano C, Colucci D'Amato L., and di Porzio U (2007). Bdnf gene is a downstream target of Nurr1 transcription factor in rat midbrain neurons in vitro. J. Neurochem 102, 441–453. [PubMed: 17506860]

Volpicelli F, De Gregorio R, Pulcrano S, Perrone-Capano C, di Porzio U, and Bellenchi GC (2012). Direct regulation of Pitx3 expression by Nurr1 in culture and in developing mouse midbrain. PLoS One 7, e30661. [PubMed: 22363463]

Wang Z, Benoit G, Liu J, Prasad S, Aarnisalo P, Liu X, Xu H, Walker NP, and Perlmann T (2003). Structure and function of Nurr1 identifies a class of ligand-independent nuclear receptors. Nature 423, 555–560. [PubMed: 12774125]

Whitehead RE, Ferrer JV, Javitch JA, and Justice JB (2001). Reaction of oxidized dopamine with endogenous cysteine residues in the human dopamine transporter. J. Neurochem 76, 1242–1251. [PubMed: 11181843]

Wirdefeldt K, Adami HO, Cole P, Trichopoulos D, and Mandel J (2011). Epidemiology and etiology of Parkinson's disease: a review of the evidence. Eur. J. Epidemiol 26 Suppl 1, S1–58. [PubMed: 21626386]

Xi Y, Noble S, and Ekker M (2011). Modeling neurodegeneration in zebrafish. Curr. Neurol. Neurosci. Rep 11, 274–282. [PubMed: 21271309]

Zetterstrom RH, Solomin L, Jansson L, Hoffer BJ, Olson L, and Perlmann T (1997). Dopamine neuron agenesis in Nurr1-deficient mice. Science 276, 248–250. [PubMed: 9092472]

Zetterstrom RH, Solomin L, Mitsiadis T, Olson L, and Perlmann T (1996). Retinoid × receptor heterodimerization and developmental expression distinguish the orphan nuclear receptors NGFI-B, Nurr1, and Nor1. Mol. Endocrinol 10, 1656–1666. [PubMed: 8961274]

Zhan YY, Chen Y, Zhang Q, Zhuang JJ, Tian M, Chen HZ, Zhang LR, Zhang HK, He JP, Wang WJ, et al. (2012). The orphan nuclear receptor Nur77 regulates LKB1 localization and activates AMPK. Nat. Chem. Biol 8, 897–904. [PubMed: 22983157]

Zhang L, Le W, Xie W, and Dani JA (2012a). Age-related changes in dopamine signaling in Nurr1 deficient mice as a model of Parkinson's disease. Neurobiol. Aging 33, 1001 e1007–1016.

Zhang Y, Nguyen DT, Olzomer EM, Poon GP, Cole NJ, Puvanendran A, Phillips BR, and Hesselson D (2017). Rescue of Pink1 Deficiency by Stress-Dependent Activation of Autophagy. Cell Chem Biol 24, 471–480 e474. [PubMed: 28366621]

Zhang Z, Li X, Xie WJ, Tuo H, Hintermann S, Jankovic J, and Le W (2012b). Anti-parkinsonian effects of Nurr1 activator in ubiquitin-proteasome system impairment induced animal model of Parkinson's disease. CNS Neurol. Disord. Drug Targets 11, 768–773. [PubMed: 22483304]

Zucca FA, Segura-Aguilar J, Ferrari E, Munoz P, Paris I, Sulzer D, Sarna T, Casella L, and Zecca L (2017). Interactions of iron, dopamine and neuromelanin pathways in brain aging and Parkinson's disease. Prog. Neurobiol 155, 96–119. [PubMed: 26455458]

Highlights

- The dopamine metabolite 5,6-dihydroxyindole (DHI) binds directly to Nurr1.
- DHI forms a covalent adduct with Nurr1, reacting as the indolequinone with Cys566.
- The Nurr1-metabolite structure reveals a previously unreported ligand binding pocket.
- DHI stimulates the transcription of Nurr1 target genes underlying dopamine homeostasis.

SIGNIFICANCE

Dysregulation of dopamine homeostasis contributes to Parkinson's disease (PD). The nuclear receptor Nurr1 plays a central role in dopamine homeostasis, regulating the transcription of genes governing the synthesis, packaging, and reuptake of dopamine. Efforts to capitalize on Nurr1's potential as a therapeutic target for PD have been hampered by the absence of a defined ligand-binding pocket within the receptor. We found that the dopamine metabolite 5,6-dihydroxyindole (DHI) binds to Nurr1 within a non-canonical pocket, forming a covalent adduct as the 5,6-indolequinone (IQ) with Cys566. In functional assays, DHI stimulates Nurr1 activity, upregulating the transcription of several genes, including the vesicular monoamine transporter 2. These results suggest that Nurr1 may be regulated by an endogenous metabolite, contradicting previous suggestions that it has no small molecule regulation.

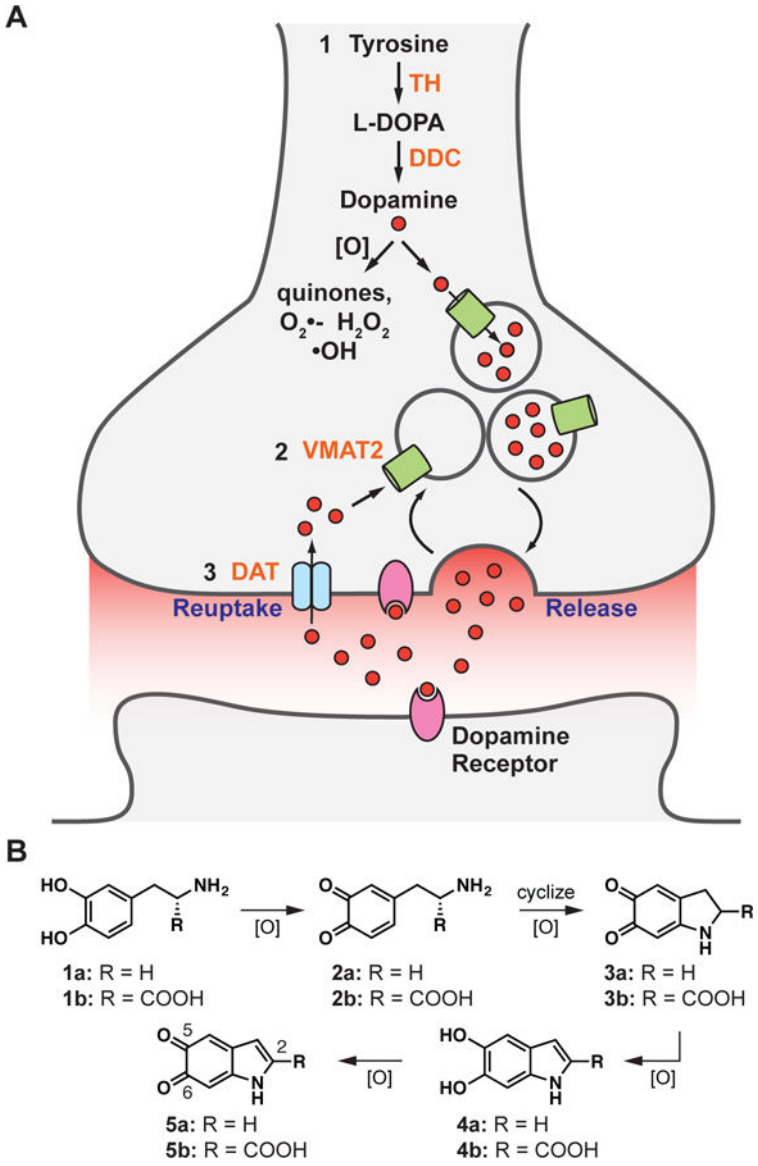

Figure 1.

The production and processing of dopamine in neurons. **(A)** Nurr1 controls the dopaminergic phenotype, regulating the genes required for the (1) synthesis (TH, DDC), (2) packaging (VMAT2), and (3) reuptake (DAT) of dopamine. **(B)** Dopamine and L-DOPA auto-oxidize to form reactive indoles and other reactive oxygen species. Only the analogs 1a, 1b, 4a, and 4b are commercially available. 1a = dopamine, 1b = L-DOPA; 2a = dopamine-o-quinone, 2b = dopaquinone; 3a = dopaminochrome, 3b = DOPAchrome; 4a = 5,6-dihydroxyindole (DHI), 4b = 5,6-dihydroxyindole-2-carboxylic acid (DHICA); 5a = 5,6-indolequinone (IQ), 5b = 5,6-dihydroxyindolequinone-2-carboxylic acid (IQCA).

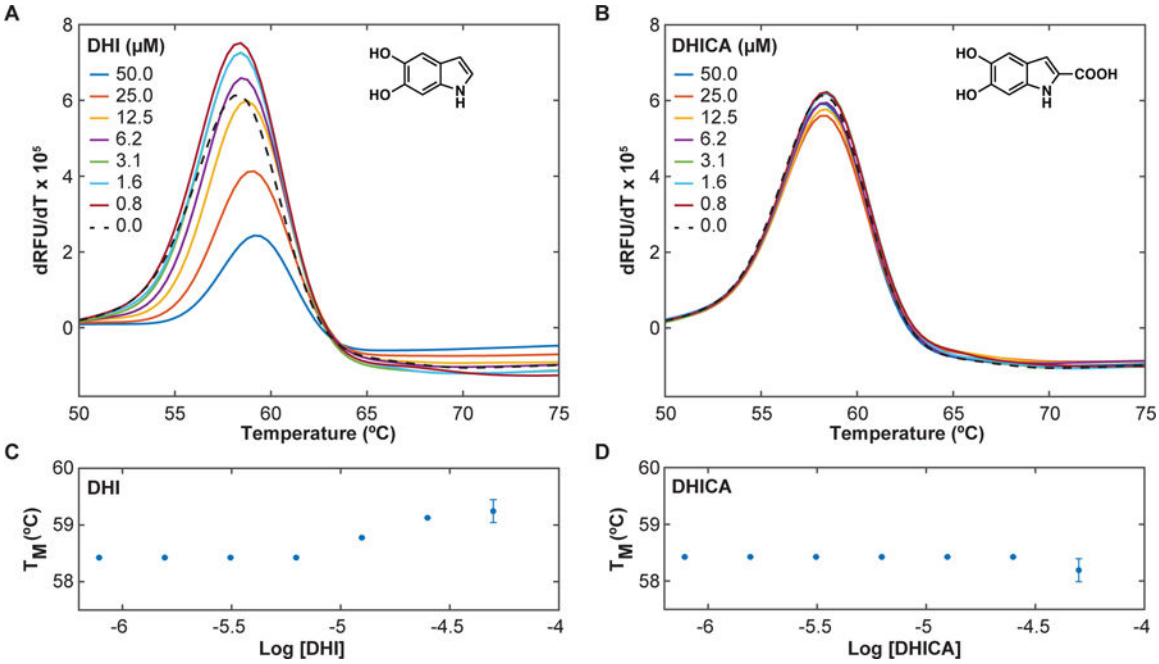

Figure 2.

DHI but not DHICA thermodynamically stabilizes the Nurr1 LBD. DSF assays were carried out on the Nurr1 LBD (4 μM) in the presence of the dye SYPRO orange (2.5x) and varying concentrations of DHI or DHICA. DHI, but not DHICA, produces a concentration-dependent increase in the Tm. **(A, B)** Plot of the temperature-derivative of the fluorescence signal versus temperature (dRFU/dT vs temperature), for (A) DHI and (B) DHICA, where the maximum (peak) of the derivative plot identifies the Tm. **(C, D)** Plot of the change in Tm as a function of the concentration of (C) DHI and (D) DHICA. Experiments were performed in triplicate. Error bars are standard deviations from three independent experiments. See also Figure S1.

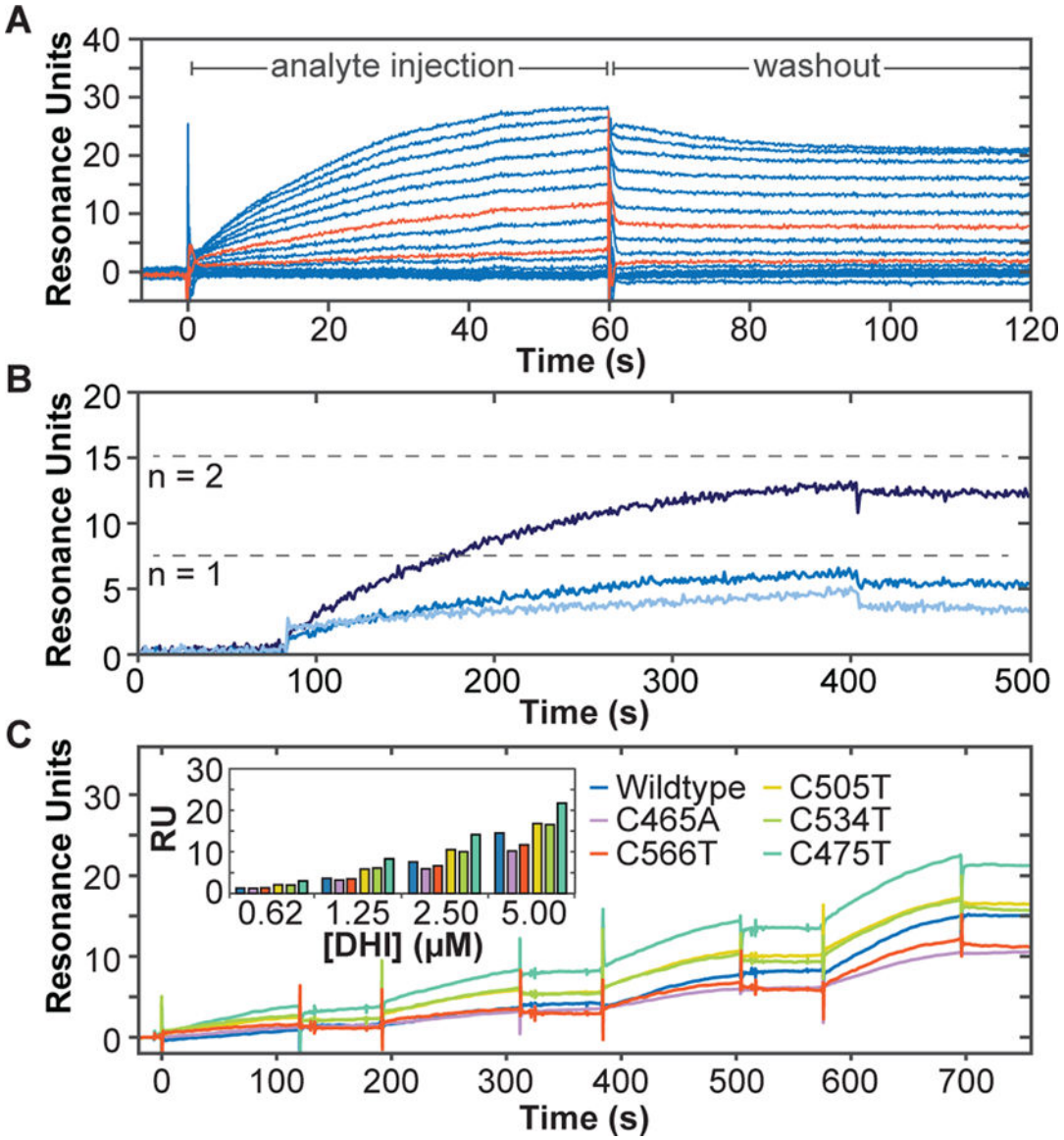

Figure 3.

Direct association of DHI with the Nurr1 LBD measured by surface plasmon resonance. Biotinylated Nurr1 LBD was coupled to a streptavidin-coated biosensor chip and exposed to DHI at varying concentrations, either without (A, C) or with (B) surface regeneration between DHI exposures. **(A)** Concentration-dependent association of DHI with Nurr1 LBD. DHI was injected at 15 increasing concentrations (16.8 μM DHI, 0.6x dilutions down to 0.01 μM; 60 s association time). DHI injections at 0.17 and 0.78 μM are highlighted in orange. **(B)** Concentration-dependent association of DHI with Nurr1 LBD (0.025, 0.25, 2.5 μM DHI; 320 s association time), with surface regeneration between DHI injections. Dashed lines indicate theoretical Rmax for a 1:1 (n =1) or 1:2 (n = 2) DHI:Nurr1 ratio. **(C)** Concentration- and time-dependent association of DHI with Nurr1 wildtype and each of five cysteine mutants. DHI was injected at four increasing concentrations (0.62, 1.25, 2.50, 5.00 μM; 120 s association time, 60 s dissociation time). Raw responses were normalized to the initial

protein captured. **(Inset)** Bar graph comparing plateau responses for each protein at the four DHI concentrations tested. See also Figure S2.

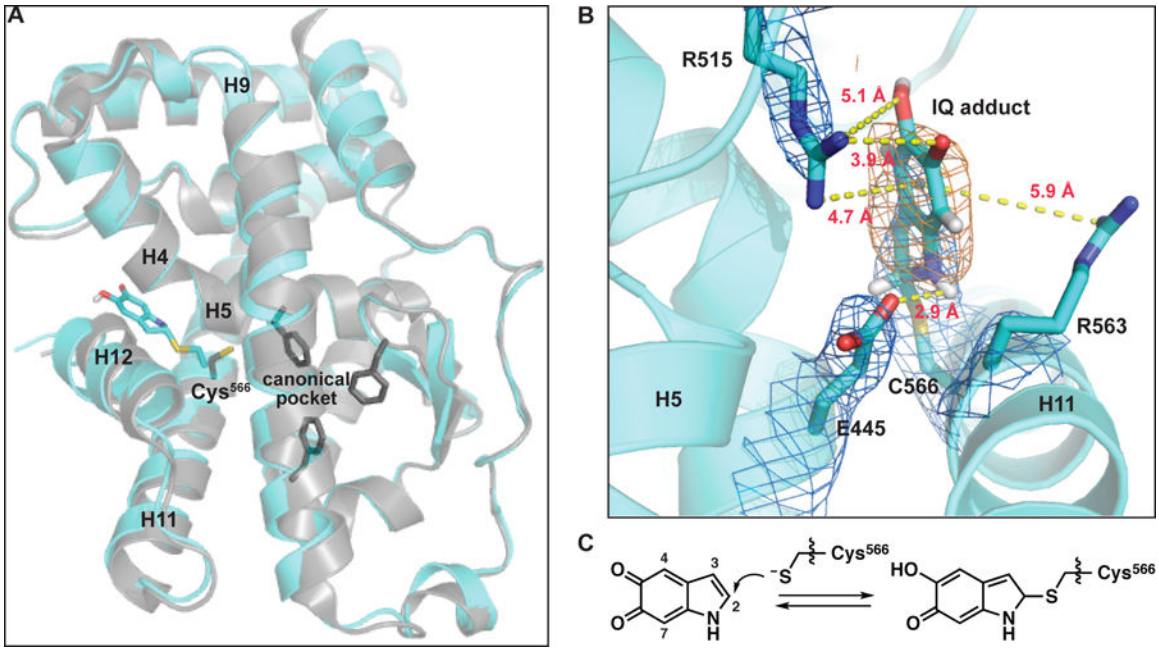

Figure 4.

Crystal structure of 5,6-indolequinone bound to the Nurr1 LBD. **(A)** Structural alignment of the IQ-bound structure (cyan; PDB: 6DDA, chain B) with the apo structure (grey, PDB: 1OVL, chain B) using H1 and H7 peptide backbone atoms for alignment. The C-alpha RMSD calculated across the entire ligand binding domain using this alignment is 1.16 Å. Shown as sticks: Cys566 IQ adduct (cyan), Cys566 from the apo structure (grey), residues in the apo structure that fill the canonical ligand binding pocket (Phe447, Phe464, Phe479; grey). **(B)** IQ forms a covalent adduct with Cys566. Depicted adduct corresponds to IQ linked at the C2 atom to Nurr1. Electron density map (2mFo-DFc, contoured to 1σ) indicated with blue mesh. Polder difference map (orange mesh) is contoured to 4.5σ in strength. Polar interactions between the Cys566 IQ adduct and Glu445 and Arg515 are highlighted; dashed yellow lines indicate distances between non-hydrogen atoms. Potential cation-pi interactions between the ligand and Arg515 and/or Arg563 are also indicated with dashed yellow lines. Weak electron density for Arg563 suggests it is dynamic. **(C)** Chemical reaction between Cys566 and IQ leading to adduct formation. See also Figures S3, S4 and S5, and Tables S1, S2, and S3.

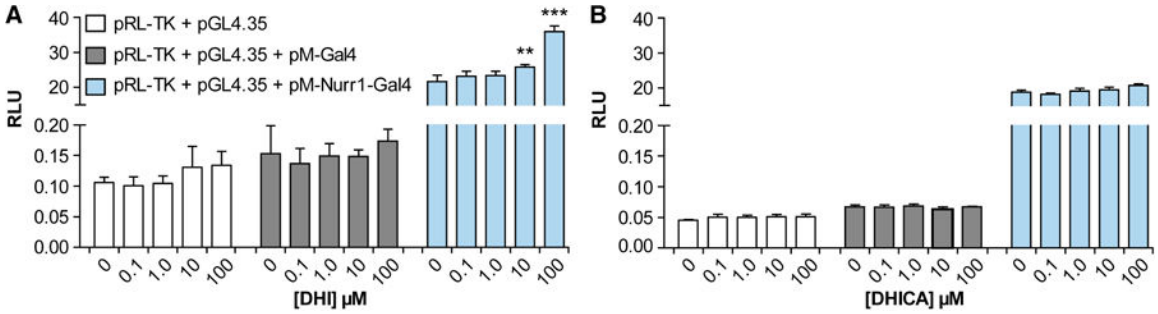

Figure 5.

DHI stimulates Nurr1 mediated transcription. JEG3 cells were co-transfected with an internal control plasmid (pRL-TK) expressing renilla luciferase, a reporter plasmid (pGL4.35) encoding the firefly luciferase gene driven by an upstream 9xGal4 element, and an expression plasmid encoding the Nurr1 LBD fused to the Gal4 DBD (pM-Nurr1-Gal4) or the Gal4 DBD alone (pM-Gal4). Cells were incubated with varying concentrations of **(A)** DHI or or **(B)** DHICA for 6 h before measuring the luciferase signal (RLU: relative luminometer units). Results are from four independent experiments. Relative average response ± SD; **p < 0.01, ***p < 0.001 by One-way Analysis of Variance (ANOVA), in comparison to response with 0 μM compound (DMSO only).

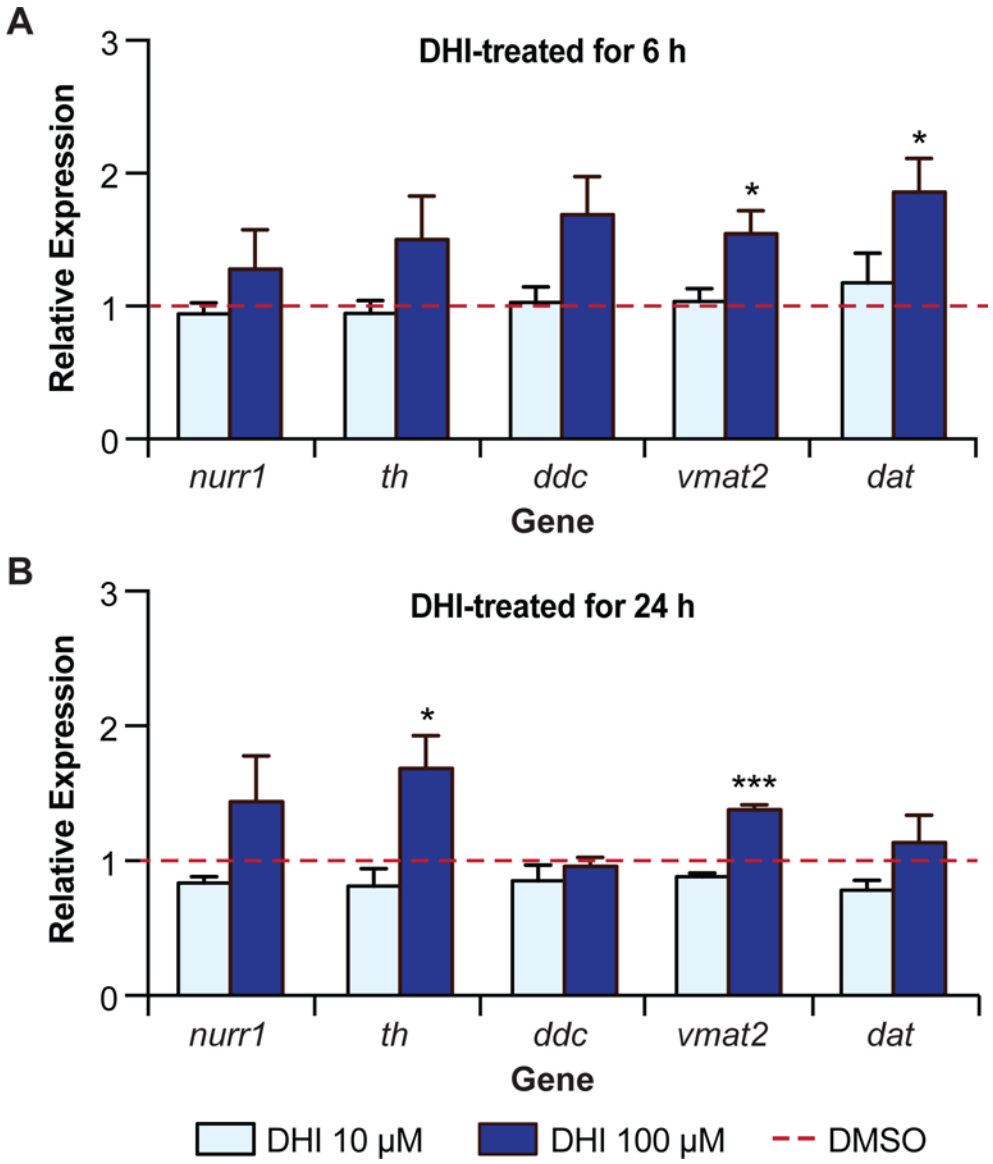

Figure 6.

DHI drives the transcription of a subset of Nurr1-dependent genes in zebrafish. **(A)** qPCR analysis of mRNA from wildtype zebrafish larvae 78 hpf following 6 h treatment with DHI (100 µM) show statistically significant increases in transcripts of *vmat2* and *dat* compared to DMSO control (red bar). **(B)** qPCR analysis of mRNA from wildtype zebrafish larvae 96 hpf after 24 h of DHI (100 µM) treatment show statistically significant increases in transcripts of *th* and *vmat2* compared to DMSO control (red bar). Transcript levels for target genes were normalized to the housekeeping gene *elf1a* and fold change was compared to gene expression levels from DMSO-treated larvae. Results are from four independent experiments. Relative average expression ± SEM; *p < 0.05, **p < 0.01, ***p < 0.001 by Student's t-test in comparison expression with 0 µM compound (DMSO only). See also Table S5.

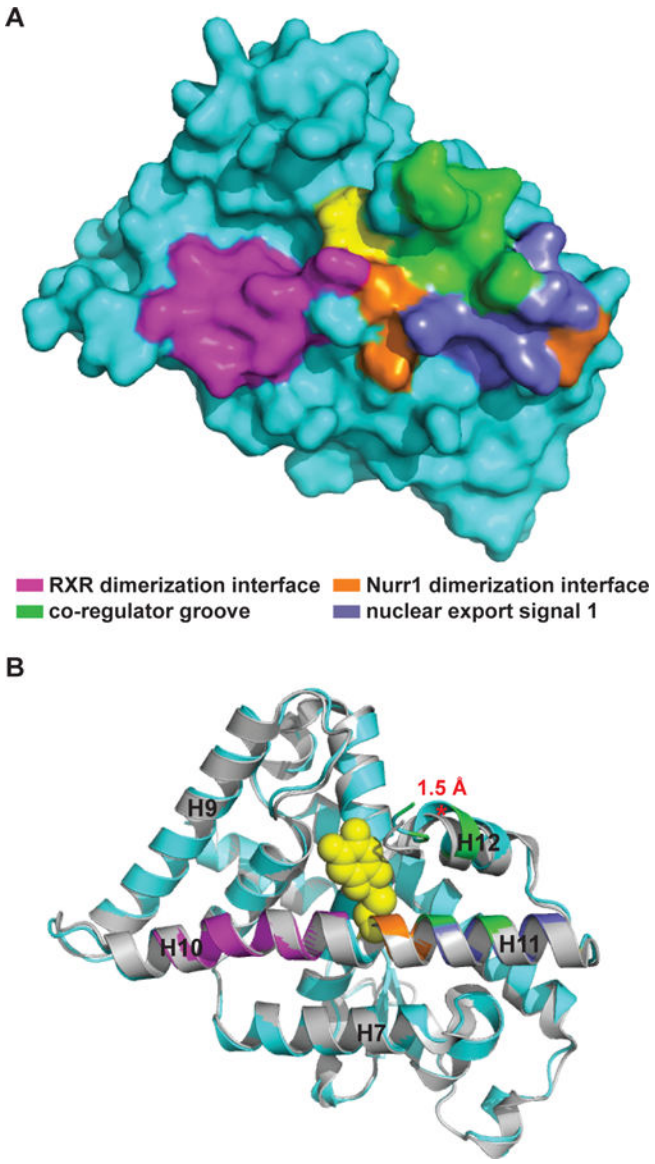

Figure 7.

The DHI/IQ binding site is situated between key regulatory elements of Nurr1 function. Cys566-IQ adduct shown as yellow spheres. **(A)** Surface rendering of the Nurr1-IQ structure highlighting the relationship between the bound metabolite and the RXR heterodimerization interface (magenta), Nurr1 homodimerization interface (orange), co-regulator groove (green), and nuclear export signal 2 (slate). **(B)** Superposition of the liganded Nurr1 structure (cyan) with the apo structure (grey), highlighting the shift (red asterisk*) between alpha-carbon residues at the end of H12 in the two structures. Nurr1 poses are identical in (A) and (B). Alignment is identical to that described for Figure 4a. See also Figure S6.